

Internal Tidal Hydrodynamics and Ambient Characteristics of the Adriatic (ITHACA)

Report on the first year of work

Principal investigator:

Mirko Orlic¹

Co-principal investigators:

Gordana Beg Paklar²

Vlado Dadic²

Nenad Leder³

Participants:

Branka Grbec²

Hrvoje Mihanovic³

Miroslava Pasaric¹

Zoran Pasaric¹

¹Andrija Mohorovicic Geophysical Institute, Faculty of Science, University of Zagreb, Croatia

²Institute of Oceanography and Fisheries, Split, Croatia

³Hydrographic Institute of the Republic of Croatia, Split, Croatia

Zagreb – Split, December 2005

DISTRIBUTION STATEMENT A
Approved for Public Release
Distribution Unlimited

Table of contents

1. Introduction	3
2. Climatological conditions in the middle Adriatic	4
2. 1. Background	4
2. 2. Atmospheric forcing	5
2. 3. Seasonal and interannual variability of temperature and salinity	9
2. 3. 1. Split-Gargano transect	9
2. 3. 2. Stoncica station	12
3. Analytical modeling of internal tides	18
3. 1. Two-layer analytical model with a step-like topography	18
3. 2. Progressive surface wave propagating from deep into shallow water	22
3. 3. Standing surface wave	30
3. 3. 1. Classical boundary conditions at the closed and open end of the basin for the surface and internal mode	35
3. 3. 2. Classical boundary conditions for the surface mode and radiation boundary condition for the internal mode at the closed and open end of the basin	42
3. 4. Discussion	48
4. Summary and conclusion	52
References	55

1. INTRODUCTION

Project “Internal Tidal Hydrodynamics and Ambient Characteristics of the Adriatic (ITHACA)” concentrates on diurnal internal tides – their generation at the Adriatic shelf break, propagation across the Palagruza Sill and dependence on stratification and currents in the area. Systematic oceanographic measurements started in 1950s at the Split-Gargano transect by the Institute of Oceanography and Fisheries (Split) and in 1960s in a wider area by the Hydrographic Institute (Split). It was found that the area is under the strong influence of seasonal and interannual variability. Early short-term current measurements revealed a pronounced seasonal signal, with oppositely directed alongshore flow in the winter and summer seasons (*Zore-Armanda*, 1968). Seasonally dependent circulation contributes to a strong temporal variability of thermohaline properties (*Grbec and Morovic*, 1997). Since the beginning of 1980s long-term current measurements were occasionally performed, showing barotropic-like current reversals on scales of a few days (*Leder et al.*, 1996). More recently, higher-frequency phenomena attracted some interest. In particular, it has been found that during the stratified season, diurnal internal tides are generated by the interaction of diurnal barotropic tides with topography and that they result in thermocline variability with amplitudes reaching 3 m (*Mihanovic*, 2005). No indications were found of semidiurnal internal tides, probably because the semidiurnal tidal currents have a minimum at the shelf break. As the detection of internal tides was based solely on data collected by three thermistors on the island of Lastovo, and there were no current measurements to support the finding, an intention of the present project is to provide a more complete data set, which would enable propagation characteristics of internal waves to be determined, not just their amplitudes. Attention is also paid to the way changes of background stratification and currents modify internal waves, and vice versa – to a possible influence of internal waves on deductions based on measurements that are scattered in space and time. Thus, observations and modeling are planned so as to enable the following hypotheses to be tested:

- Diurnal surface tides generate internal tidal waves at the Adriatic shelf break.
- Internal tidal energy radiates away from the shelf break. Some waves travel towards the northwest, thus crossing the Palagruza Sill.
- Generation and propagation of baroclinic waves is influenced by stratification and currents prevailing in the area.

The project started on 12 April 2005 with the financial support of the USA Office of Naval Research (award No. N00014-05-1-0698) and the Croatian Ministry of Science, Education and Sports (contract No. 3/2005) and is expected to last until 30 September 2007. Preparation of the field work is planned for the first year, execution of the experiment for the second year, and analysis of the data and model results for the third year.

This is report on the first year of work on the project, which – following the project proposal – concentrated on the preparations for the field work by (1) analyzing historical data collected in the Palagruza Sill area and (2) developing a simple model that approximates the Adriatic shelf break with a depth discontinuity and basin stratification with two layers.

2. CLIMATOLOGICAL CONDITIONS IN THE MIDDLE ADRIATIC

2. 1. Background

The earliest oceanographic research of the Adriatic Sea started already in the 19th century. However, systematic and regular measurements in the middle Adriatic began in 1950s by the Institute of Oceanography and Fisheries in Split. One of the most investigated areas in the middle Adriatic is the Split-Gargano transect (Figure 1), region characterized by a strong temporal variability of thermohaline structure determined by a number of factors: interaction between the atmosphere and sea leading e. g. to deep water formation in the north Adriatic, river discharge, water exchange through the Otranto Strait and topographic effect of the Palagruza Sill (*Zore-Armanda and Bone, 1987*).

Generally, current outflows from the Adriatic to the Mediterranean in the bottom layer, whereas the Mediterranean water enters the Adriatic in the intermediate layer. In winter, in the north Adriatic, very cold dense water is formed, whereupon it sinks to deep layers of the Jabuka Pit and is occasionally advected across the Palagruza Sill (*Zore-Armanda, 1963*). The transect area is also under the influence of saltier water advected from the south Adriatic and from the Mediterranean. Advection of the Mediterranean water, called "ingression" (*Buljan, 1974*), brings Mediterranean saltier water into the Adriatic, causing a strong increase of salinity in the middle Adriatic. Since the temperature of Levantine Intermediate Water (LIW) is higher than that of the Adriatic water, "ingressions" are also manifested as an increase of temperature (*Zore-Armanda, 1969a*). Additionally, ingressions cause increase in nutrients and consequently enhance primary production. Relating these phenomena to the climate, *Zore-Armanda (1969b)* stated that the most important factor enhancing the water exchange between the two basins is the horizontal air pressure gradient over the east Mediterranean. The locations of the Iceland cyclone and Siberian anticyclone centers were found to control the air pressure differences over the Adriatic (*Zore-Armanda, 1969c*). It was found that such changes could be related to conditions in a wider area of the north Atlantic and Europe (*Grbec et al., 2003*).

The Palagruza Sill transect is exposed to a number of different impacts, which makes it suitable for investigation of specific thermohaline features on both the seasonal and interannual scales (e.g. *Orlic et al., 1992; Grbec and Morovic, 1997; Grbec, 1998; Zore-Armanda et al., 1999*).

In the following, atmospheric forcing in the middle Adriatic is briefly considered. Hydrographic conditions are then described by presenting thermohaline features observed along the Palagruza transect, which also comprises Stoncica – the station best investigated in the region.

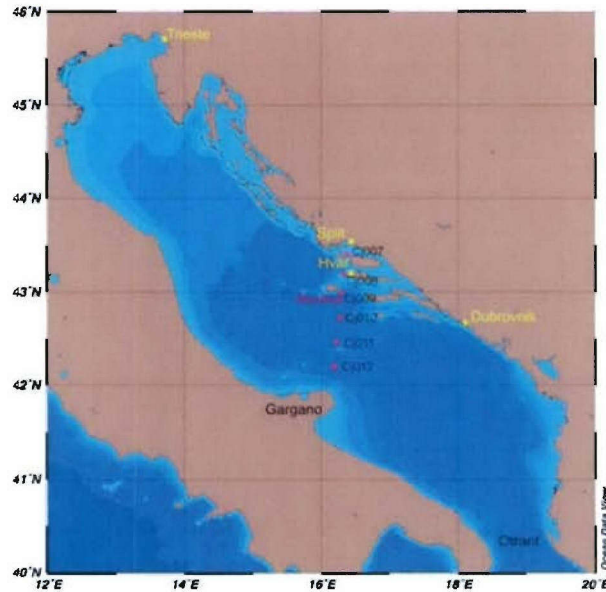


Figure 1. Map of the Adriatic showing bathymetry of the basin and position of permanent meteorological stations and stations CJ07 – CJ12 of the Split-Gargano transect.

2. 2. Atmospheric forcing

The middle Adriatic is located in the area in which strong orographic effects of Dalmatian mountains modify weather conditions whereas the climate has almost Mediterranean features. Strong cyclonic activity over the Adriatic, especially in the cold part of year, causes different weather types to occur (Penzar, 1967; Loncar and Bajic, 1994) with frequent exchange of Sirocco and Bora events (Figure 2). During summer, this area is under the influence of subtropical high-pressure belt, so warm and dry conditions prevail with well-developed sea-land breeze systems. Seasonal variations of main atmospheric parameters such as solar radiation, wind, air temperature and precipitation cause strong seasonal variability of heat and water flux between the atmosphere and the sea (Figures 3-5).

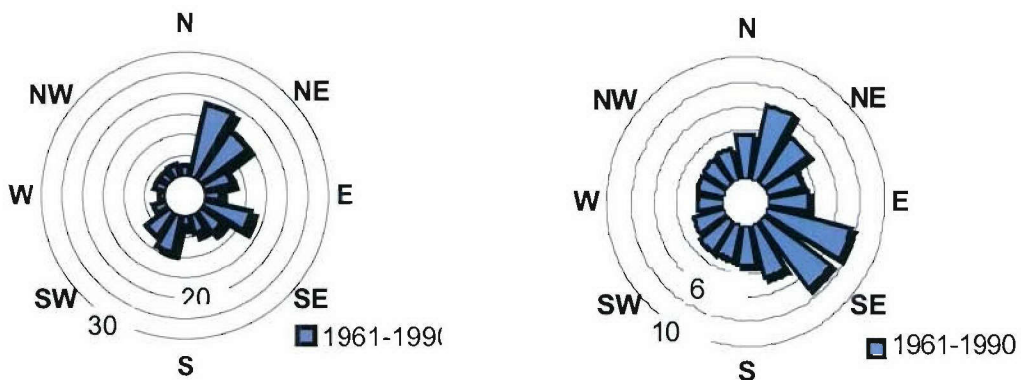


Figure 2. Annual wind roses (relative frequency of wind directions, *left*, and average wind velocities, *right*) according to wind measurements at the Split-Marjan station over the 1961-1990 interval.

The annual cycle of heat flux is controlled by heat gain due to incoming short-wave radiation and heat losses through outgoing long-wave radiation, evaporation and conduction of heat. These components of heat flux for the middle Adriatic were estimated using different semi-empirical equations (*Grbec et al., 1997*) using data originating from surface meteorological stations distributed along the east Adriatic coast (*Grbec, 1998; Matic, 2005*). After several automatic meteorological stations were established, short-wave radiation and long-wave backward radiation were measured directly (ADRICOSM reports, 2002-2003).

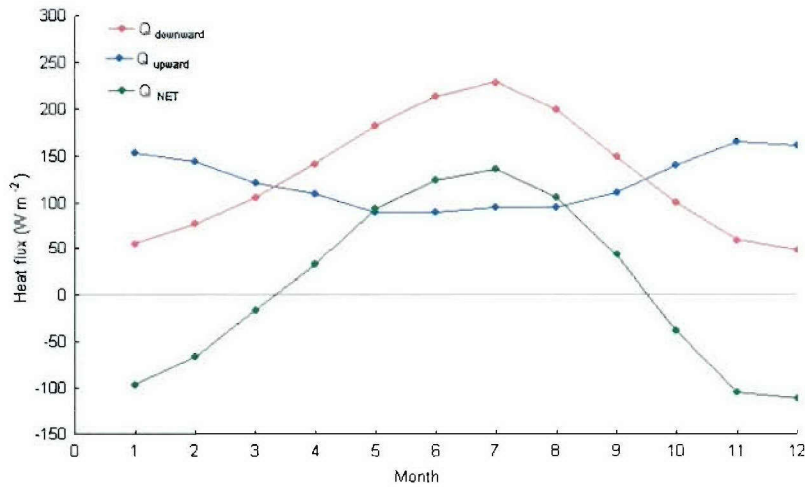


Figure 3. Seasonal cycle of upward, downward and net heat flux obtained from measurements performed at Split-Marjan over the 1961-1990 interval.

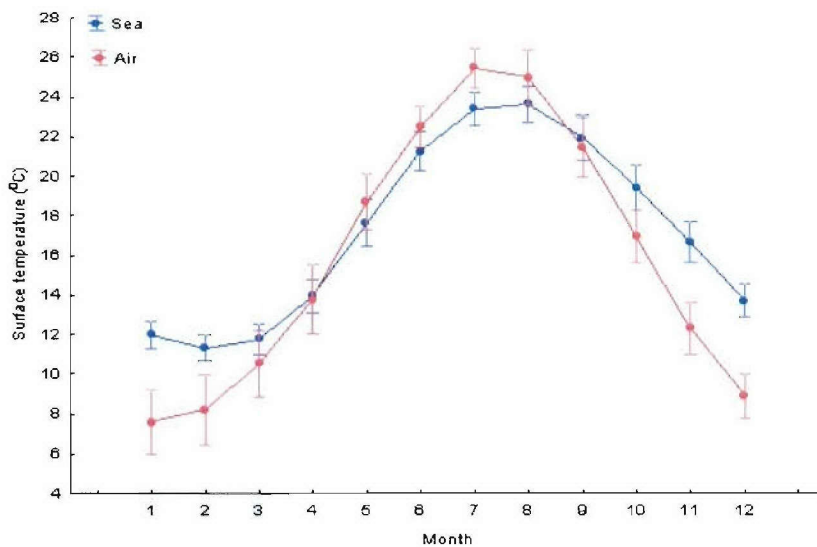


Figure 4. Seasonal cycles of surface air and sea temperature at the meteorological station Split-Marjan, for the 1961-1990 interval. Vertical bars represent standard deviations.

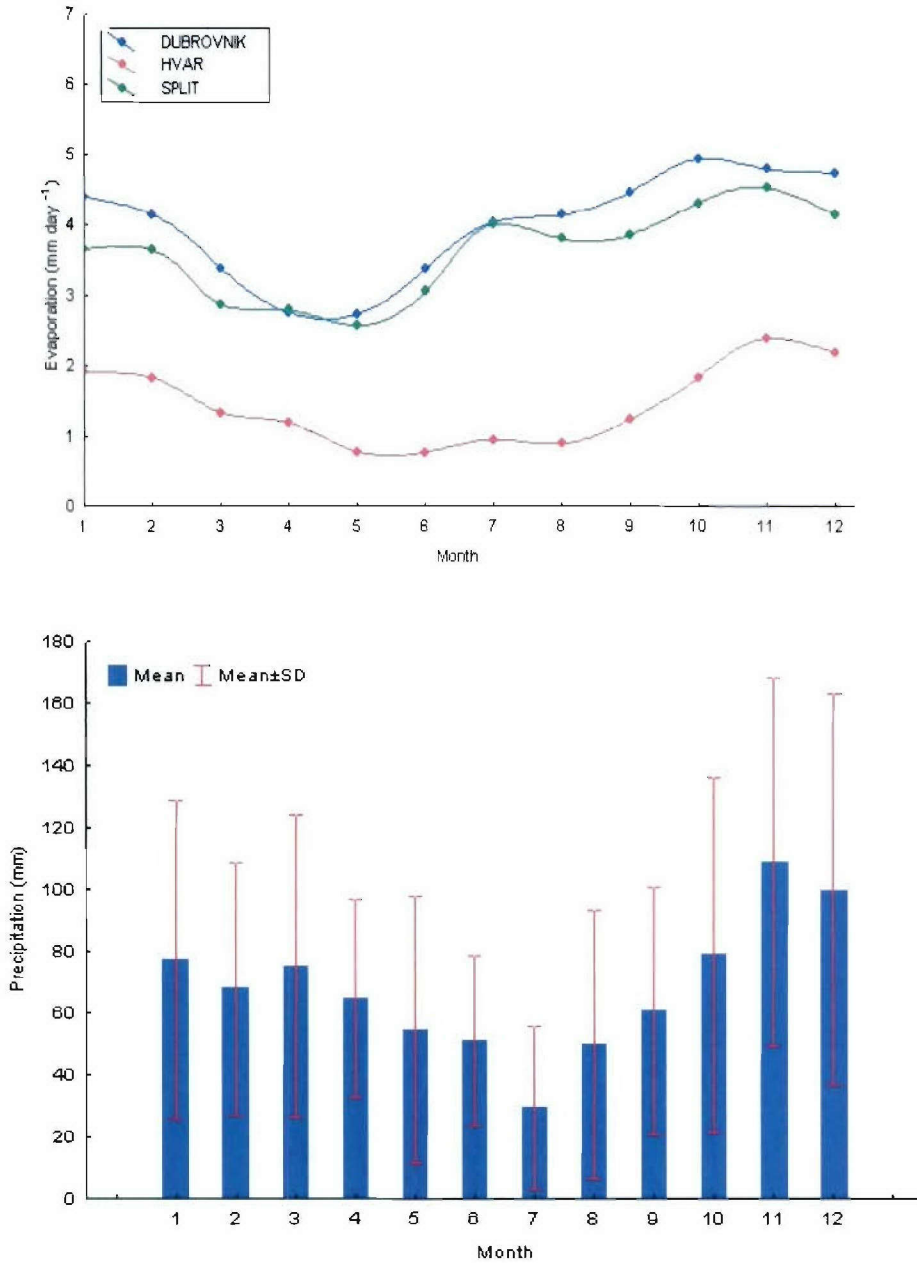


Figure 5. Seasonal cycle of evaporation for various stations along the east Adriatic coast (*top*) and precipitation at the meteorological station Split-Marjan (*bottom*), for the 1961-1990 interval. Vertical bars represent standard deviations.

Mean seasonal net heat flux cycle (Figure 3) shows that from April to September the sea receives heat from the atmosphere, reaching maximum in July (134.6 Wm^{-2} at station Split-Marjan). The sea loses heat most strongly in December (112.1 Wm^{-2} at station Split-Marjan); at the annual scale the loss of heat is caused by long-wave radiation (60%), evaporation (33%) and much less by conduction (7%). Correspondingly, from May until August the sea is colder and from October until March the sea is warmer than the overlaying atmosphere (Figure 4).

Water exchange at the air-sea interface, determined using monthly mean values from meteorological stations Dubrovnik, Hvar and Split, is shown in Figure 5. Evaporation at different stations along the coast is considerably different from that at the open sea, both in annual courses and in absolute values. Evaporation along the east Adriatic coast reaches maximum in cooling season, with the values far from the coast (meteorological station Hvar) being significantly lower than those close to the coast. Fresh water input by precipitation decreases while going towards the open sea, since there is no orographic effect which is considerable near the coast. Therefore, due to various influences, mean seasonal P-E cycles differ significantly for the coastal and the open middle Adriatic area.

It is interesting to note that during extreme weather conditions (Table 1), for example during strong Bura events, the heat loss from the sea is extremely high, causing cooling of the sea surface and gradual salinity increase due to strong evaporation.

In addition to the strong seasonal cycles in the atmospheric and boundary layer parameters, long-term increasing/decreasing trends can be detected which highlight the changeable middle Adriatic climate. These changes are clearly reflected in the long-term variability of hydrographic properties as, for example, sea surface temperature (Figure 6).

Table 1. Mean daily values of heat flux components (W/m^2) during several extreme weather events at the meteorological station Split-Marjan. Q_s denotes shortwave radiation, Q_H is sensible heat flux, Q_E is latent heat flux, Q_L is longwave heat flux, and Q_{NET} is net heat flux at the air-sea interface. T_A and T_S , in $^{\circ}C$, denote surface air- and sea-temperature, respectively.

CASE	WIND SPEED (ms^{-1}) DIRECTION	CLOUDINESS C/10	RELATIVE HUM. %	TA TS	QS	QH	QE	QL	QNET
					(W m^{-2})				
02 JAN 1979	NNE 19.9	0.6	33	-4.3 12.6	57	420	508	164	-1035
08 JAN 1981	NNE 16.9	0	37	-1.9 12.0	96	327	434	166	-831
02 DEC 1983	NNE 16.9	1	36	+1.4 13.5	39	283	471	127	-842

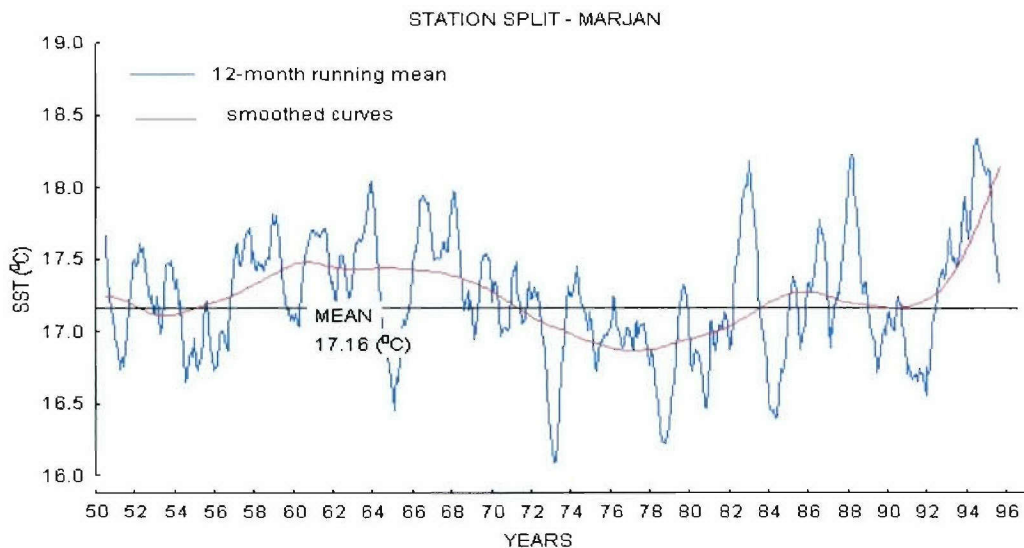


Figure 6. Long-term sea surface temperature (SST) fluctuations obtained from twice-daily measurements at the Split-Marjan station.

2. 3. Seasonal and interannual variability of temperature and salinity

2. 3. 1. Split-Gargano transect

Thermohaline variations over the year at the Split-Gargano transect are a result of different processes in the surface and deeper layers, causing presence of particular water masses in different seasons, as seen from T-S diagrams (Figure 7). Different thermohaline features observed from May 1998 to May 1999 at the Split-Gargano transect are analyzed and compared with average water mass characteristics for the region.

The figures presented describe thermohaline properties in the middle Adriatic in 1998 and 1999. In winter 1999, enhanced heat loss and low Po River discharge resulted in the North Adriatic Dense Water (NAdDW) formation, in contrast to winter 1998 when, due to weak air-sea exchange and moderate Po River discharge, fresh water was present in the whole north Adriatic and consequently the NAdDW was not formed (Zore-Armanda et al., 1999; Vilibic et al., 2004). After the formation, NAdDW flowed as a high density current along the west Adriatic slope towards the Jabuka Pit. Its densest core interacted with the topography and rapidly sank when reaching relatively steep slope, west of the Jabuka Pit. The second part followed the slope as a high density current, but not interacting with the bottom topography, detouring the pit along its southeast side and hitting the bottom somewhere in the east segment of the pit. Changes of thermohaline properties along the Palagruza Sill are documented in Figures 8 and 9, using data collected between April 2004 and February 2005 during cruises of RV Bios (project Jadran). Close to the east Adriatic coast less

saline water is present in the surface layer during a greater part of the year. This is especially visible during maximum freshwater inflow in spring. During winter vertically homogenous water column is found in the whole transect, with temperature and salinity being lower close to the east coast. Of course, thermohaline conditions observed between April 2004 and February 2005 can be discussed only as a case study, taking into account prevailing atmospheric processes.

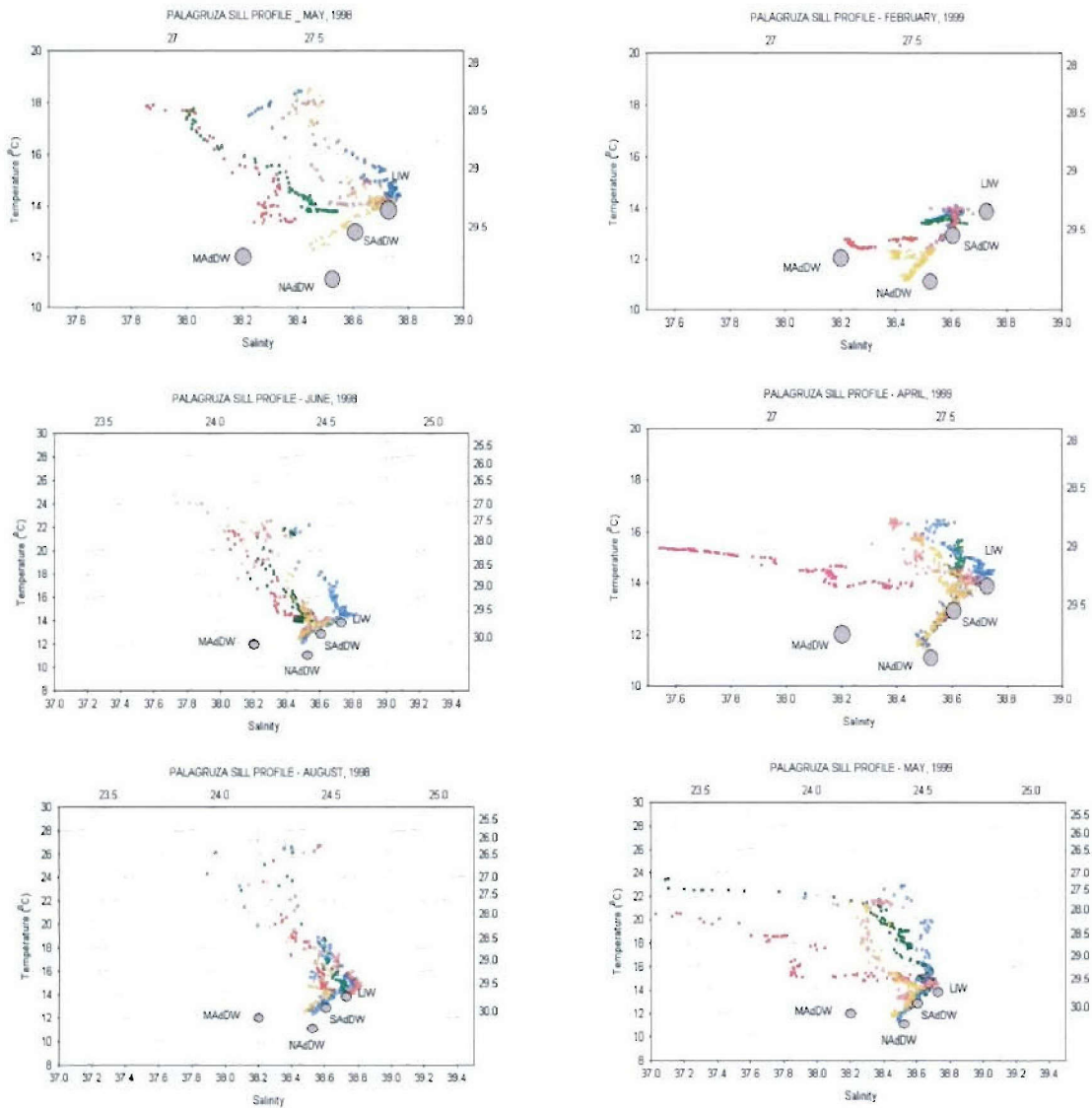


Figure 7. T-S diagrams constructed from data collected at the Split-Gargano transect between May 1998 and May 1999.

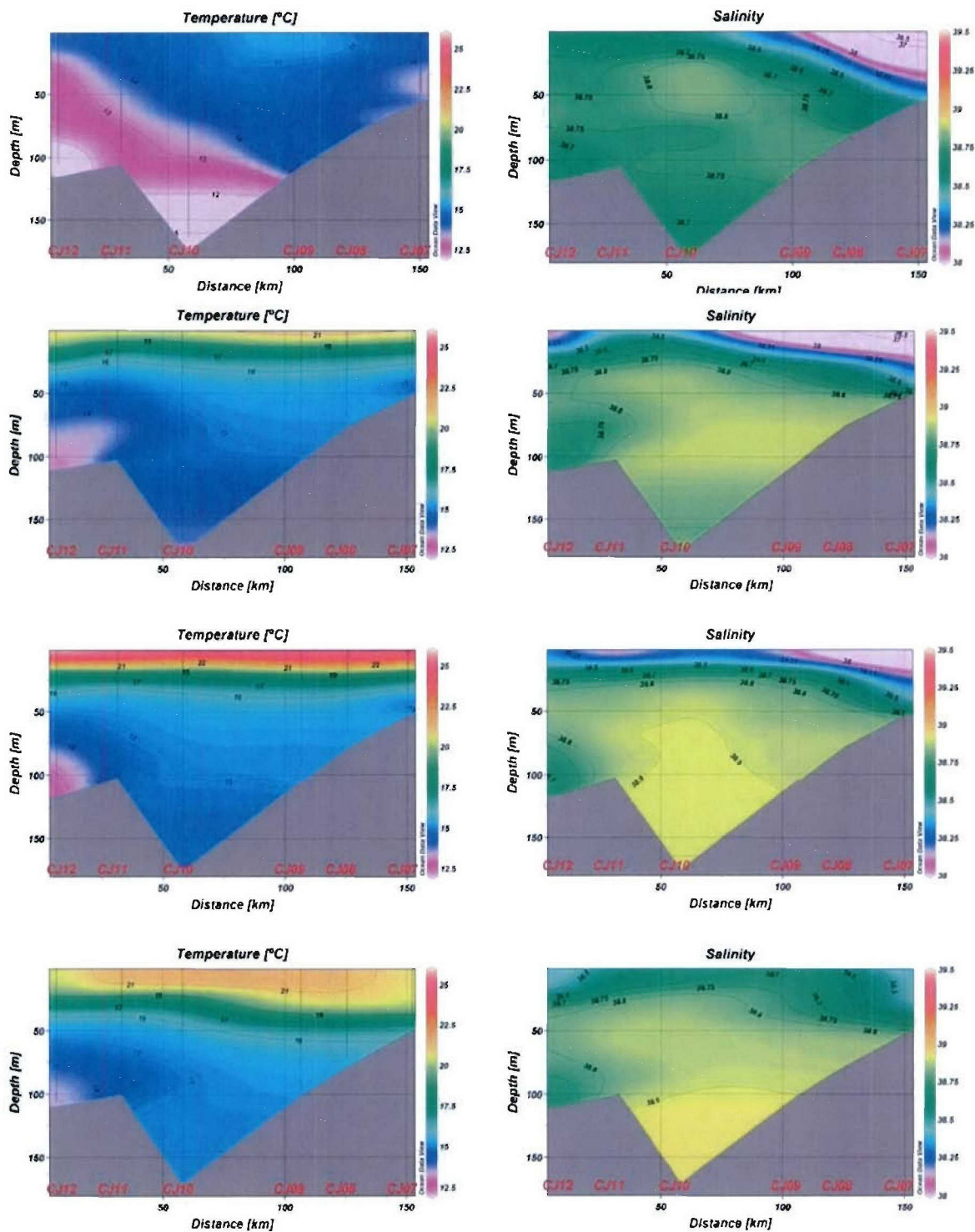


Figure 8. Distribution of temperature and salinity along the Palagruza Sill transect for April, June, July and September 2004. Gargano is on the left and Split on the right.

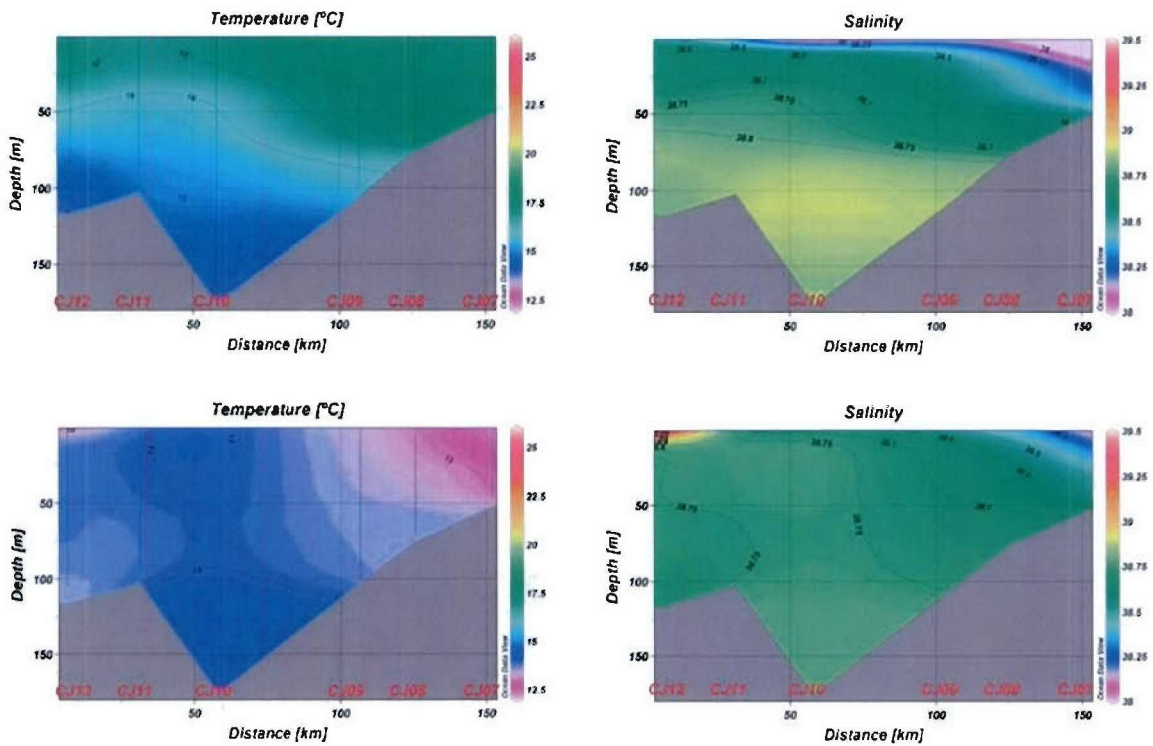


Figure 9. As in Figure 8, except for December 2004 and February 2005.

2. 3. 2. Stoncica station

Long series of monthly values of temperature and salinity, measured between January 1961 and December 1995, were used to analyze mean seasonal thermohaline features of the Vis island area. The data were collected during regular monthly cruises at the oceanographic station Stoncica (see Figure 1). Measurements were made mostly once a month (only exceptionally several times per month) at standard oceanographic depths (0, 10, 20, 30, 50, 75 and 100 m).

The mean seasonal cycle of temperature (Figure 10) is very pronounced down to 20 meter depth, with rather small temperature changes at 100 meters where temperature does not fall below 12°C. The curves show isothermal conditions at all depths in late autumn and winter, whereas stratification is present from May until October. Annual temperature maximum in the deeper layers is lagging the surface one, whereas minimum at all depths occurs within the same month. An earlier study (*Grbec*, 1998) showed that at the depth of 10 meters the temperature maximum has a delay of 9 days with respect to that in the surface layer, whereas at 20 meters the maximum is delayed 48 days. The 75 and 100 meter depths have a lag of 93 days relative to the surface. Minimum temperature in the surface layer occurs in February, and at 75 and 100 meters at the beginning of March. An interesting feature, related to temperature variations in a particular month (represented here with the standard deviation), may be observed: the largest variability during summer and early autumn is seen in the intermediate layer.

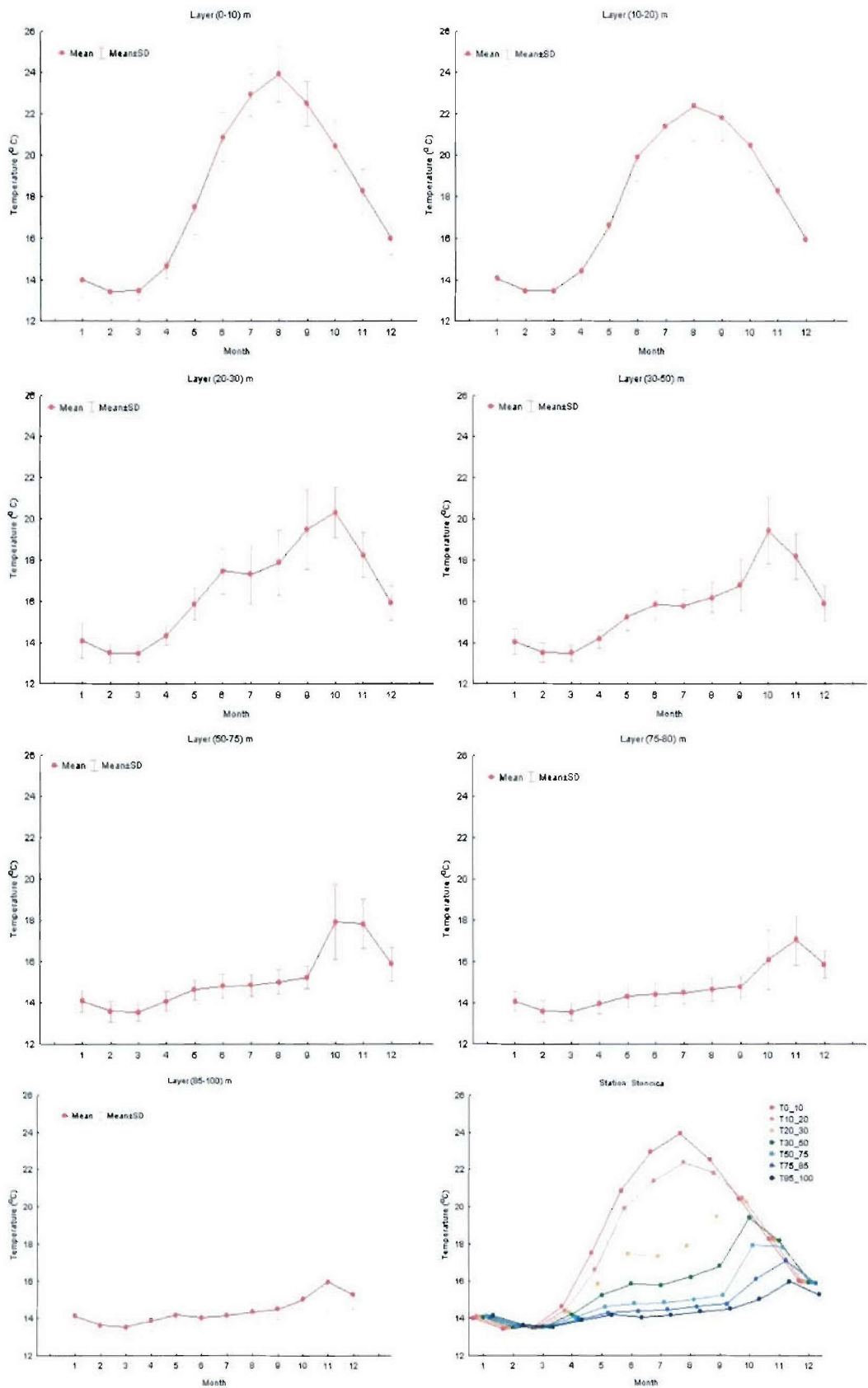


Figure 10. Mean seasonal temperature cycles for selected layers at Stoncica station.

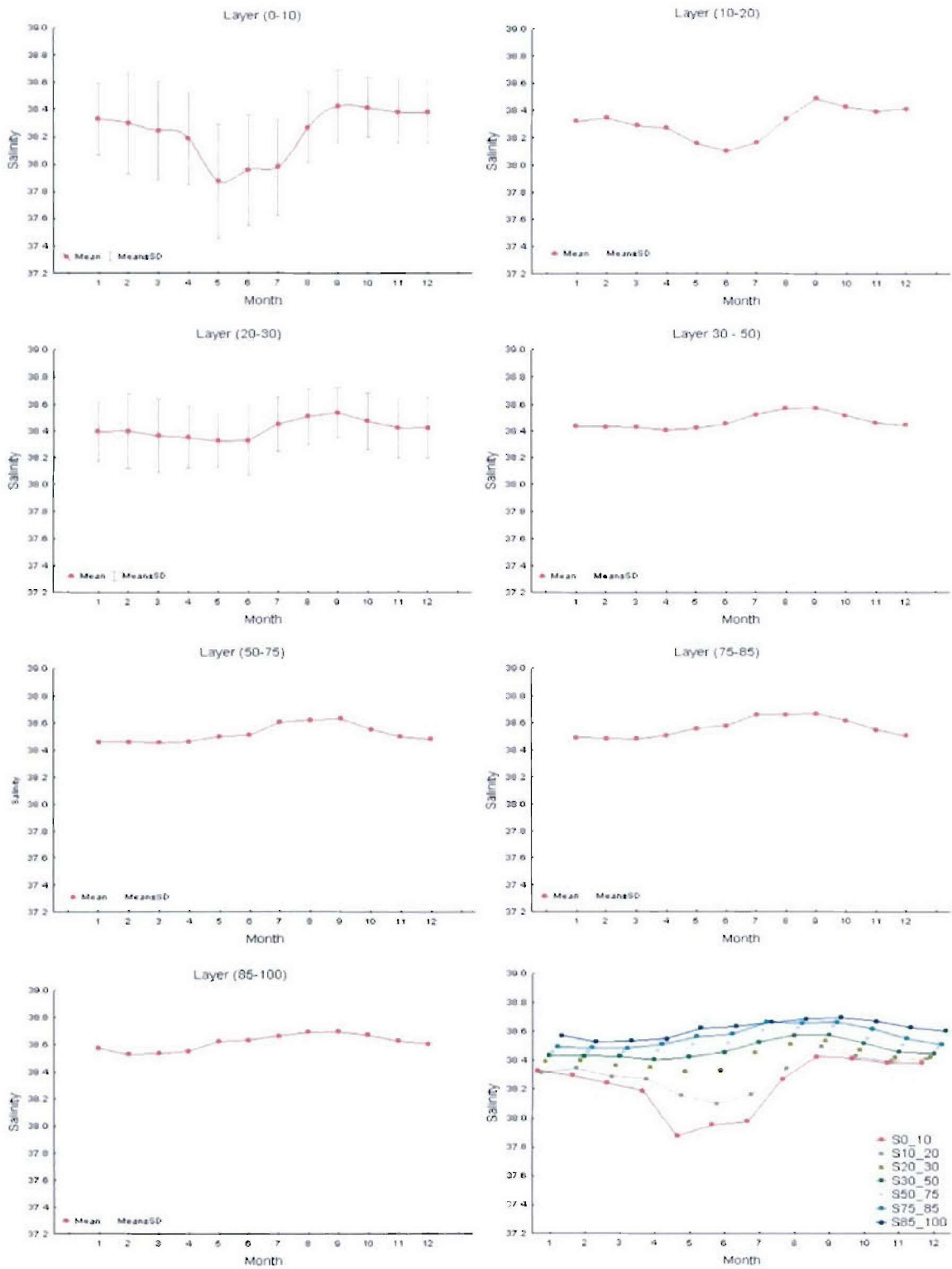


Figure 11. Mean seasonal salinity cycles for selected layers at Stoncica station.

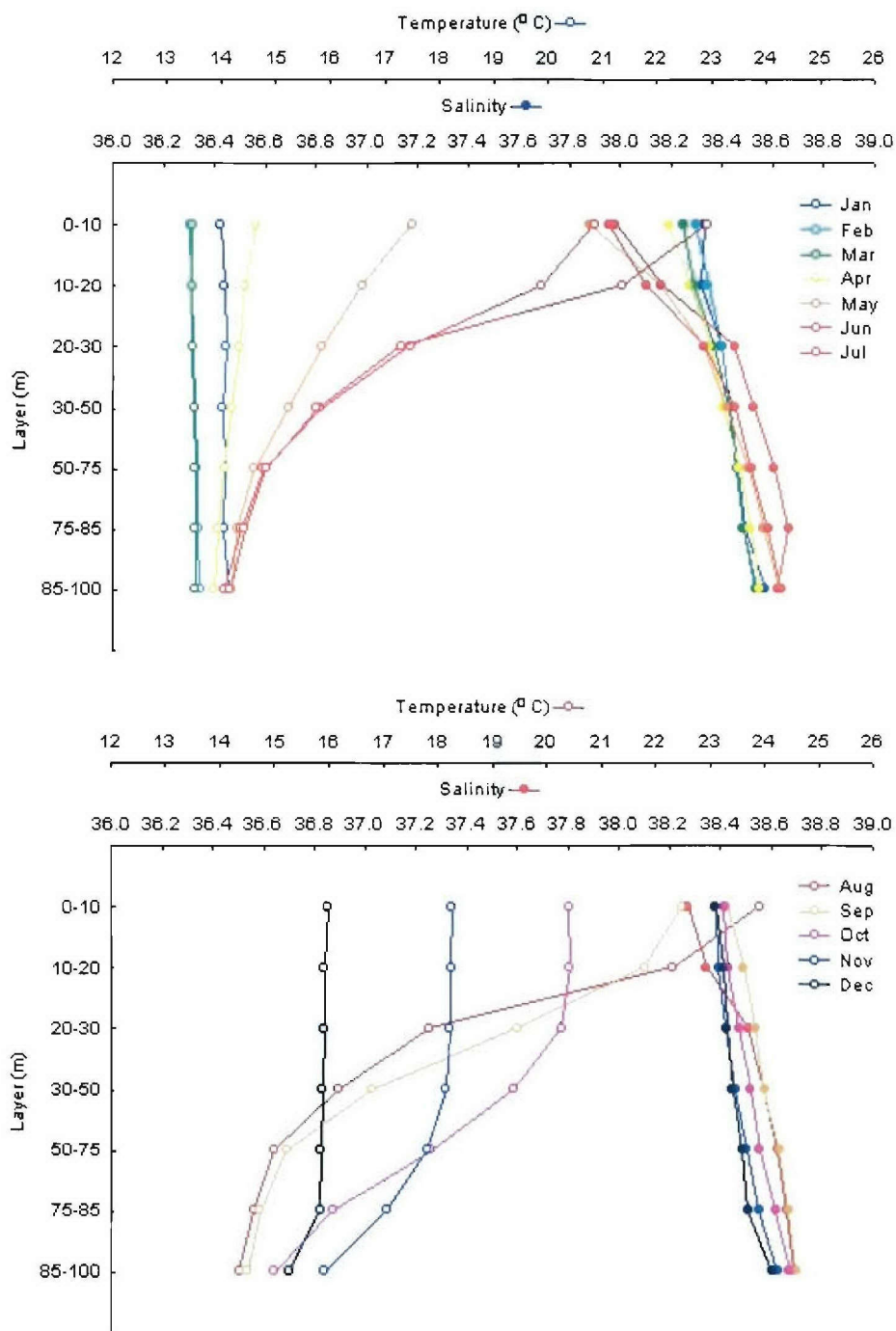


Figure 12. Mean vertical temperature and salinity profiles for Stoncica station.

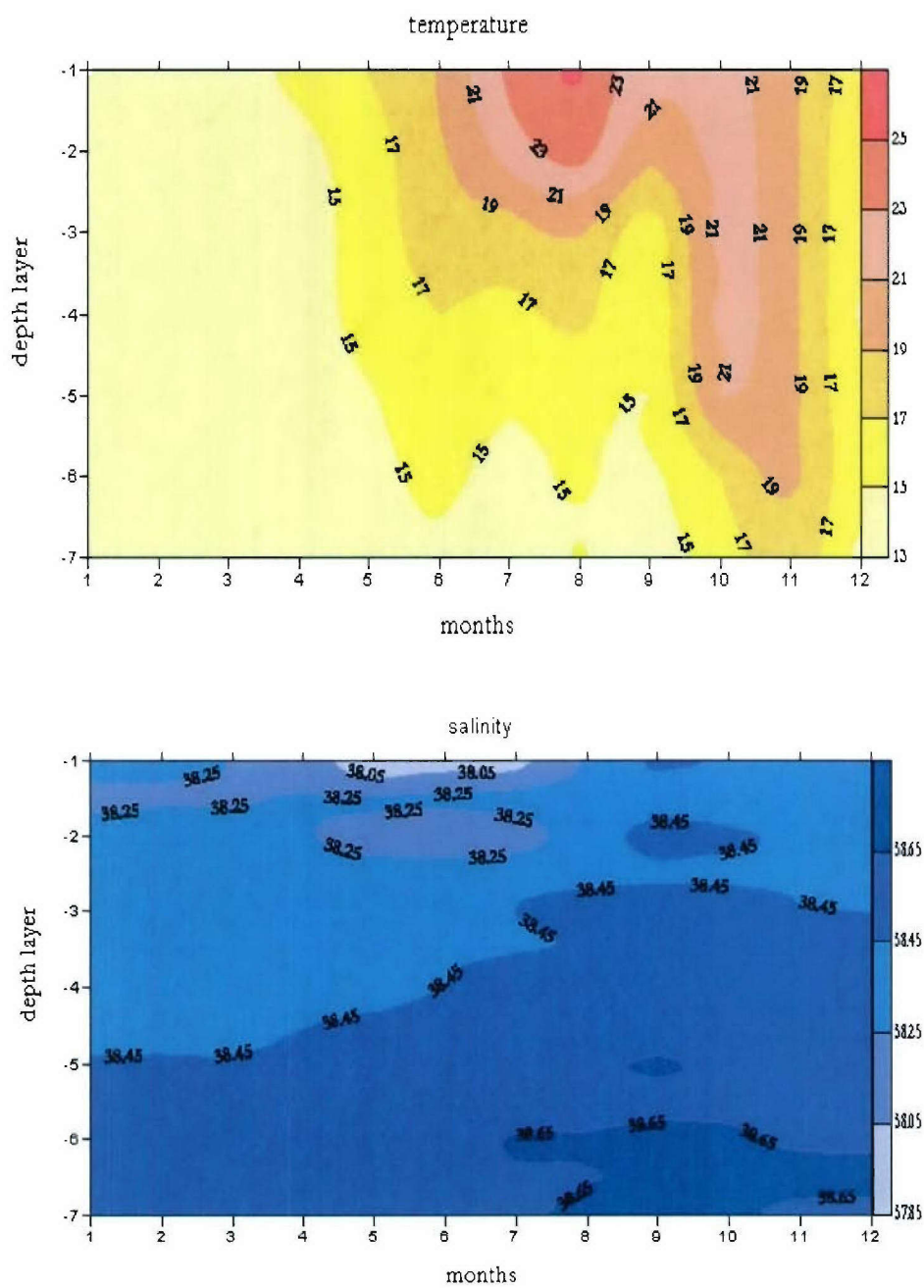


Figure 13. Time evolution of temperature and salinity obtained from monthly mean values for the Stoncica station and the 1961-1995 interval. Depth layers -1 to -7 denote layers having 0-10, 10-20, 20-30, 30-50, 50-75, 75-85 and 85-100 meter depths, respectively.

The seasonal salinity cycle (Figure 11) shows salinity increase with depth. Again, the largest seasonal variations are observed in the surface layer, whereas at greater depths salinity is more steady. In the surface layer down to 10 meters there are two minima, in May and in July. Salinity maximum is not pronounced, although larger values at all depths are observed in late summer and early autumn. The observed interannual variability is probably related to advection from the Mediterranean.

The vertical distribution of temperature shows the presence of thermocline below the 20 m depth, while the distribution of salinity shows halocline at almost the same depth (Figures 12 and 13).

In the deeper layers the maximum temperature values in May are the consequence of fast transport of heat to the layers. In summer, thermocline suppresses transport of heat to the deeper layers and, consequently, lower temperatures are observed below the thermocline throughout the summer (Figure 12). Besides the heat flux, the wind has considerable influence on temperature of the water column. Increase of wind speed in autumn coincides with the temperature increase in deeper layers, as wind induced mixing transports heat from the warm surface layers to the deeper ones.

Salinity in the surface layer during the heating season mirrors P-E values, whereas – somewhat surprisingly – in autumn and winter salinity and P-E values are in phase. When the thermocline is well developed, lighter east Adriatic surface waters reside in the surface layer and are advected to the Split-Gargano transect. They bring about a decrease of salinity in the surface layer, mixing being prevented by the fully developed thermocline. In summer, due to current system in the intermediate layer (*Zore-Armanda*, 1969b), advection of saltier water from the south Adriatic (Mediterranean) is observed (Figure 12). In the warmer part of the year the two salinity minima may be attributed to the Neretva River outflow (in May) and to the influence of the rivers outflowing from the south Adriatic coast (in July).

It is evident that vertical mixing processes have essential influence on thermohaline properties of the whole water column, but with different strength over the year. These vertical processes are to a considerable extent controlled by direct atmospheric forcing. In addition, thermohaline properties are heavily influenced by horizontal advection, which is determined by oceanographic as well as meteorological conditions.

3. ANALYTICAL MODELLING OF INTERNAL TIDES

3. 1. Two-layer analytical model with a step-like topography

The first simple analytical model describing the generation of internal tides was presented by *Rattray* (1960). He described the analysis of two-layer system with an abrupt change of topography under presumption of long waves, and showed that this model gives an amplification of internal tides with respect to surface tides. Introduction of real topography and continuous density distribution limits the possibilities of analytical modeling, making numerical approach the only possible alternative. Analytical solutions of idealized model were also considered for linear shelf slope between the coast and depth discontinuity (*Rattray*, 1960), and for linear discontinuity slope (*Prinsenbergh and Rattray*, 1975). Modal approach described by *Prinsenbergh and Rattray* (1975) is appropriate for linear shelf slope and any given stratification, whilst *Baines* (1982) presented analytical models that are applying different approach in internal tide research, based on the ray theory. Standard integral equation is solved, and solutions can be obtained for any topography but only for certain (continuous) density distributions. The greater part of models, analytical and numerical, was vertically two-dimensional (*Maze*, 1987; *Sherwin and Taylor*, 1990), but *Baines* (1986) and *Sherwin et al.* (2002) emphasize importance of 3D modeling, because of the influence of along-slope barotropic flow. Obliqueness of barotropic wave was considered by *Guizien et al.* (1999). They were following original *Rattray's* approach, with different boundary conditions at the coast. Namely, *Rattray* used wave reflection at the coast, which gave partial standing waves on the shelf, while *Guizien et al.* in their analysis of internal tide generation by surface tidal wave incoming to the shelf with certain incidence angle, used radiation boundary condition at the coast (no reflection at the solid boundary).

Analytical approach to the generation of internal tides in the vicinity of the shelf edge is relevant if certain assumptions are fulfilled. These assumptions are two-layer fluid and rapid depth change (*Guizien et al.*, 1999). Long waves and step-like topography assumptions are valid as long as wave lengths are significantly larger than shelf dimensions along rapid depth changes. The island of Lastovo, from which internal tides in the Adriatic were observed for the first time (*Mihanovic*, 2005), is located about 140 km from the center of the South Adriatic Pit, with an abrupt depth change at a distance of about 30 km. Since wave lengths of barotropic surface waves are of the order of 1000 km, it can be concluded that this assumption is satisfied. Another important supposition, which is very important for this kind of analytic models, is two-layer fluid approximation. It also implies the existence of the first mode of internal oscillations only, which is the case for the best part of shallow seas, where stratification exists when seasonal thermocline is developed (*Huthnance*, 1989). During June 2001 the most significant temperature oscillations were detected at the depth of 22 m (especially during the first half of June), and oscillations at 15 and 36 meters were not that significant (*Mihanovic*, 2005). It could be concluded that in the interval mentioned thermocline was positioned in this part of the water column. CTD measurements from August 1990 confirm typical vertical distribution of thermohaline properties of this area, with three typical layers. However, thermocline (pycnocline) was very pronounced and narrow, so vertical structure can be approximated by two-

layer system (Leder, 2002). Therefore, this assumption in a wider Lastovo area is also fulfilled.

Two-layer analytical model used in theoretical study of the generation of internal tides in the Adriatic is based on decomposed equations for barotropic and baroclinic mode of oscillations of a two-layer fluid in rotating rectangular channel (e.g. Csanady, 1971; Orlic, 1988). Traditional and hydrostatic approximations were introduced, whilst tidal forcing, nonlinear effects, lateral friction and stress at the pycnocline were neglected:

$$\begin{aligned}
 & \frac{\partial u_\rho}{\partial t} - fv_\rho = -g \frac{\partial \zeta_\rho}{\partial x} + \frac{\tau_{xs}}{(h+h')\rho} - \frac{\tau'_{xb}}{(h+h')\rho'} \\
 \text{surface} & \\
 \text{(barotropic)} & \\
 \text{mode:} & \\
 & \frac{\partial v_\rho}{\partial t} + fu_\rho = -g \frac{\partial \zeta_\rho}{\partial y} + \frac{\tau_{ys}}{(h+h')\rho} - \frac{\tau'_{yb}}{(h+h')\rho'} \\
 & (h+h') \left(\frac{\partial u_\rho}{\partial x} + \frac{\partial v_\rho}{\partial y} \right) + \frac{\partial \zeta_\rho}{\partial t} = 0
 \end{aligned} \tag{3.1}$$

$$\begin{aligned}
 & \frac{\partial u'_u}{\partial t} - f'v'_u = -g\varepsilon \frac{h}{h+h'} \frac{\partial \zeta'_u}{\partial x} - \frac{\tau_{xs}}{(h+h')\rho} - \frac{h}{h'(h+h')} \frac{\tau'_{xb}}{\rho'} \\
 \text{internal} & \\
 \text{(baroclinic)} & \\
 \text{mode:} & \\
 & \frac{\partial v'_u}{\partial t} + f'u'_u = -g\varepsilon \frac{h}{h+h'} \frac{\partial \zeta'_u}{\partial y} - \frac{\tau_{ys}}{(h+h')\rho} - \frac{h}{h'(h+h')} \frac{\tau'_{yb}}{\rho'} \\
 & h' \left(\frac{\partial u'_u}{\partial x} + \frac{\partial v'_u}{\partial y} \right) + \frac{\partial \zeta'_u}{\partial t} = 0,
 \end{aligned} \tag{3.2}$$

where ζ_ρ , u_ρ and v_ρ represent elevation and velocity components for the surface (barotropic) mode, ζ'_u , u'_u and v'_u elevation and velocity components for the internal (baroclinic) mode, ρ and h are constant density and undisturbed depth of the surface layer (thermocline depth), ρ' and h' are constant density and undisturbed depth of the bottom layer, τ_{xs} and τ_{ys} are surface stress components, and τ'_{xb} and τ'_{yb} are bottom stress components. Notation $\varepsilon = (\rho' - \rho)/\rho'$ is introduced as well.

The connection between solution for the surface mode and surface elevation and current component oscillations in the bottom layer is given by:

$$\zeta'_\rho = \frac{h'}{h+h'} \zeta_\rho; \quad u'_\rho = u_\rho; \quad v'_\rho = v_\rho,$$

while relation between the internal mode solutions and surface elevation and current component oscillations in the surface layer is given by:

$$\zeta_u = 0; \quad u_u = -\frac{h'}{h}u'_u; \quad v_u = -\frac{h'}{h}v'_u.$$

Integral solution for the surface and bottom layer can be reconstructed by combining solutions of (3.1) and (3.2):

$$\begin{aligned} \zeta &= \zeta_p + \zeta_u = \zeta_p \\ \zeta' &= \zeta'_p + \zeta'_u \\ u &= u_p + u_u \\ v &= v_p + v_u \\ u' &= u'_p + u'_u \\ v' &= v'_p + v'_u . \end{aligned} \tag{3.3}$$

Having in mind that theoretical study of internal tides in the Adriatic will be based on frictionless two-layer analytical model, variations in direction parallel to the shelf discontinuity can be neglected, together with the surface and bottom friction. Coriolis force components were usually disregarded in traditional studies of conversion of barotropic into baroclinic signal (*Miles, 1974*), which is valid for the surface mode since Rossby radius of deformation is one order of magnitude larger than spatial dimensions in which generation processes take place (*Gill, 1982*). Specifically, internal tides are generated at the edge of deeper Adriatic region, in which surface Rossby radius of deformation has an order of magnitude of about 1000 km, while generation processes take place in area of about 100 x 100 km. This argument is not valid for internal mode, since in June 2001 internal Rossby radius of deformation near Lastovo island was about 3 km (*Mihanovic, 2005*), and lengths of internal tidal waves are usually between 20 and 40 km (e.g. *Holloway, 1983, 1987; New and Da Silva, 2002*). For this reason Coriolis force has an important influence on prevention of soliton generation (solitons are nonlinear waves connected to internal tides, *Gerkema, 1996*). However, since analytical modeling described in this report is aimed at understanding the basics of internal tides in the Adriatic, Coriolis force will be discarded for both the surface and internal modes. Equations (3.1) and (3.2) then become:

$$\begin{aligned}
& \text{surface mode:} & \frac{\partial u_\rho}{\partial t} = -g \frac{\partial \zeta_\rho}{\partial x} & \zeta'_\rho = \frac{h'}{h+h'} \zeta_\rho \\
& & (h+h') \frac{\partial u_\rho}{\partial x} + \frac{\partial \zeta_\rho}{\partial t} = 0 & u'_\rho = u_\rho
\end{aligned} \tag{3.4}$$

$$\begin{aligned}
& \text{internal mode:} & \frac{\partial u'_u}{\partial t} = -g\epsilon \frac{h}{h+h'} \frac{\partial \zeta'_u}{\partial x} & \zeta_u = 0 \\
& & h' \frac{\partial u'_u}{\partial x} + \frac{\partial \zeta'_u}{\partial t} = 0 & u_u = -\frac{h'}{h} u'_u.
\end{aligned} \tag{3.5}$$

Elevation and velocity in the surface and bottom layer are:

$$\begin{aligned}
\zeta &= \zeta_\rho + \zeta_u = \zeta_\rho \\
\zeta' &= \zeta'_\rho + \zeta'_u = \frac{h'}{h+h'} \zeta_\rho + \zeta'_u \\
u &= u_\rho + u_u = u_\rho - \frac{h'}{h} u'_u \\
u' &= u'_\rho + u'_u = u_\rho + u'_u.
\end{aligned}$$

General expression for surface mode elevation will be $\zeta_\rho = A_\rho \exp[i(\omega t \pm k_\rho x)]$, and for internal mode elevation $\zeta'_u = A'_u \exp[i(\omega t \pm k'_u x)]$. By combining equations (3.4) and (3.5), wave equation for the surface and internal mode is obtained:

$$\begin{aligned}
& \text{surface mode:} & \frac{\partial^2 \zeta_\rho}{\partial t^2} = g(h+h') \frac{\partial^2 \zeta_\rho}{\partial x^2} \\
& \text{internal mode:} & \frac{\partial^2 \zeta'_u}{\partial t^2} = g\epsilon \frac{hh'}{h+h'} \frac{\partial^2 \zeta'_u}{\partial x^2},
\end{aligned}$$

which for the assumed wave forms give connection between wave number and angular frequency:

$$\begin{aligned} \text{surface mode:} \quad k_p^2 &= \frac{\omega^2}{g(h+h')} \\ \text{internal mode:} \quad k_u'^2 &= \frac{\omega^2(h+h')}{g\epsilon h h'}. \end{aligned}$$

By introducing notations for periodic speed and elevation of the surface and internal mode of oscillations, and by using equations (3.4) and (3.5), relationship between current speed and elevation of the surface and internal mode is found:

$$u = \tilde{u} \exp(i\omega t) \quad ; \quad \zeta = \tilde{\zeta} \exp(i\omega t) ;$$

and

$$\begin{aligned} \text{surface mode:} \quad u_p &= i \frac{g}{\omega} \frac{d\tilde{\zeta}_p}{dx} \exp(i\omega t) \\ \text{internal mode:} \quad u_u' &= i \frac{g\epsilon h}{\omega(h+h')} \frac{d\tilde{\zeta}_u'}{dx} \exp(i\omega t). \end{aligned} \tag{3.6}$$

3. 2. Progressive surface wave propagating from deep into shallow water

Results of two-layer analytical model, allowing for an abrupt depth change at the shelf break and assuming progressive wave propagating from deep into shallow water, will be considered. Schematic presentation of the model is given in Figure 14. Since model area has two parts with different bottom layer depths and same thermocline depth, notation in equations for the surface and internal mode is slightly changed. Apostrophe which was denoting influence of internal mode on the surface and bottom layer will be replaced by “-” for negative x and “+” for positive x . The same notation will be used in the surface mode equations.

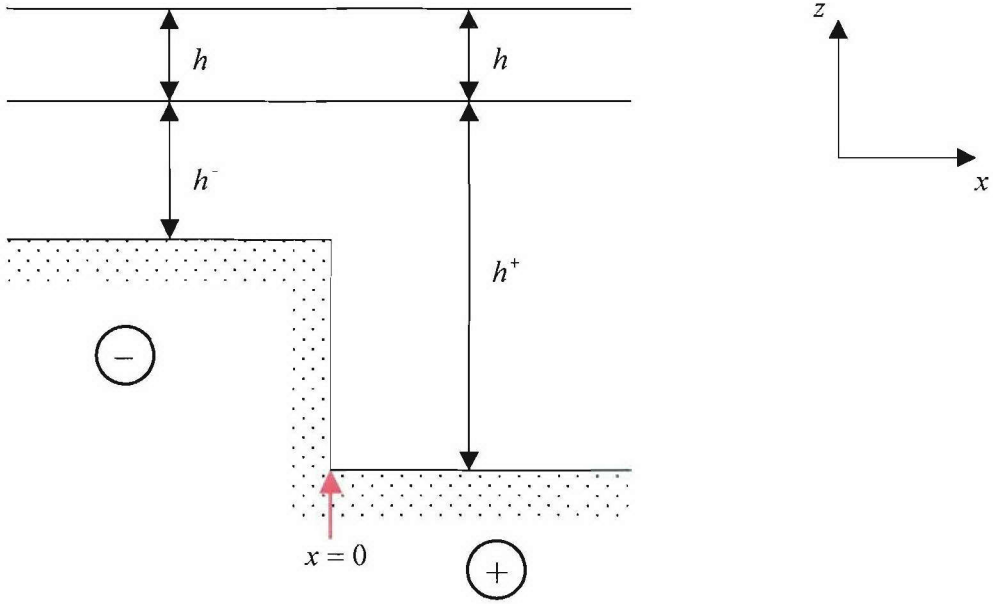


Figure 14. Schematic presentation of idealized topography for two-layer analytical model with shelf region (-) and deep sea region (+) indicated.

If an incoming wave with amplitude I_p propagates from region (+) into region (-), abrupt topography change generates reflected barotropic wave in (+), transmitted barotropic wave in (-), reflected baroclinic wave in (+) and transmitted baroclinic wave in (-):

$$\begin{aligned}
 & \text{surface mode:} \\
 & \zeta_p^- = T_p^- \exp[i(\omega t + k_p^- x)] \\
 & \zeta_p^+ = I_p \exp[i(\omega t + k_p^+ x)] + R_p^+ \exp[i(\omega t - k_p^+ x)] \\
 & \text{internal mode:} \\
 & \zeta_u^- = T_u^- \exp[i(\omega t + k_u^- x)] \\
 & \zeta_u^+ = R_u^+ \exp[i(\omega t - k_u^+ x)] ,
 \end{aligned} \tag{3.7}$$

where T_p^- represents transmitted barotropic wave amplitude in region (-), R_p^+ is amplitude of reflected barotropic wave in region (+), T_u^- denotes transmitted baroclinic wave amplitude in region (-) and R_u^+ reflected baroclinic wave amplitude in region (+).

Relationship between speed and elevation of the surface and internal mode can be found on the basis of equations (3.6):

$$u_{\rho}^{-} = -\frac{g}{c_{\rho}^{-}} T_{\rho}^{-} \exp[i(\omega t + k_{\rho}^{-} x)]$$

surface mode:

$$u_{\rho}^{+} = -\frac{g}{c_{\rho}^{+}} \{I_{\rho} \exp[i(\omega t + k_{\rho}^{+} x)] - R_{\rho}^{+} \exp[i(\omega t - k_{\rho}^{+} x)]\}$$

(3.8)

$$u_{u}^{-} = -\frac{G^{-}}{c_{u}^{-}} T_{u}^{-} \exp[i(\omega t + k_{u}^{-} x)]$$

internal mode:

$$u_{u}^{+} = \frac{G^{+}}{c_{u}^{+}} R_{u}^{+} \exp[i(\omega t - k_{u}^{+} x)],$$

with:

$$c_{\rho}^{-} = \sqrt{g(h+h^{-})} ; \quad c_{\rho}^{+} = \sqrt{g(h+h^{+})} ;$$

$$c_{u}^{-} = \sqrt{G^{-} h^{-}} ; \quad G^{-} = g\varepsilon \frac{h}{h+h^{-}} ; \quad c_{u}^{+} = \sqrt{G^{+} h^{+}} ; \quad G^{+} = g\varepsilon \frac{h}{h+h^{+}} .$$

Wave forms for the surface and internal mode in region (-) and region (+) include four unknown amplitudes which depend on the amplitude of incoming surface wave. Relationship between these amplitudes can be obtained by using boundary conditions at depth discontinuity. At $x = 0$, elevation continuity in the surface and bottom layer, along with continuous flow in the entire water column and in the surface layer, needs to be fulfilled. Expressions (3.4) and (3.5) are also taken into account, showing the influence of the surface mode elevation on the bottom layer elevation, and of the internal mode speed on speed in the surface layer. Boundary conditions are then:

$$\zeta_{\rho}^{-} = \zeta_{\rho}^{+} \quad (3.9a)$$

$$\frac{h^{-}}{h+h^{-}} \zeta_{\rho}^{-} + \zeta_{u}^{-} = \frac{h^{+}}{h+h^{+}} \zeta_{\rho}^{+} + \zeta_{u}^{+} \quad (3.9b)$$

$$u_{\rho}^{-}(h+h^{-}) = u_{\rho}^{+}(h+h^{+}) \quad (3.9c)$$

$$u_{\rho}^{-} - \frac{h^{-}}{h} u_{u}^{-} = u_{\rho}^{+} - \frac{h^{+}}{h} u_{u}^{+} . \quad (3.9d)$$

If expressions (3.7) and (3.8) are included in boundary conditions (3.9) for $x = 0$, four equations with five variables are obtained. In this way, unknown amplitudes of

reflected and transmitted waves can be expressed in terms of amplitude of the incoming surface wave. System of equations is as follows:

$$T_{\rho}^{-} = I_{\rho} + R_{\rho}^{+} \quad (3.10a)$$

$$\frac{h^{-}}{h+h^{-}} T_{\rho}^{-} + T_u^{-} = \frac{h^{+}}{h+h^{+}} [I_{\rho} + R_{\rho}^{+}] + R_u^{+} \quad (3.10b)$$

$$\frac{h+h^{-}}{c_{\rho}^{-}} T_{\rho}^{-} = \frac{h+h^{+}}{c_{\rho}^{+}} [I_{\rho} - R_{\rho}^{+}] \quad (3.10c)$$

$$\frac{g}{c_{\rho}^{-}} T_{\rho}^{-} - \frac{h^{-}}{h} \frac{G^{-}}{c_u^{-}} T_u^{-} = \frac{g}{c_{\rho}^{+}} [I_{\rho} - R_{\rho}^{+}] + \frac{h^{+}}{h} \frac{G^{+}}{c_u^{+}} R_u^{+} . \quad (3.10d)$$

From (3.10a) and (3.10c), which are the same equations as in barotropic case (Cerovecki, 1992), one could get:

$$R_{\rho}^{+} = \frac{c_{\rho}^{+} - c_{\rho}^{-}}{c_{\rho}^{-} + c_{\rho}^{+}} I_{\rho} = \frac{\sqrt{H^{+}} - \sqrt{H^{-}}}{\sqrt{H^{-}} + \sqrt{H^{+}}} I_{\rho} \quad (3.11)$$

$$T_{\rho}^{-} = \frac{2c_{\rho}^{+}}{c_{\rho}^{-} + c_{\rho}^{+}} I_{\rho} = \frac{2\sqrt{H^{+}}}{\sqrt{H^{-}} + \sqrt{H^{+}}} I_{\rho} ,$$

where $H^{-} = h+h^{-}$ and $H^{+} = h+h^{+}$, i.e. depths of shallow and deep region respectively.

Including these terms in equations (3.10b) and (3.10d), system of equations for R_u^{+} and T_u^{-} is found. From (3.10b):

$$T_u^{-} = \frac{h^{+}}{h+h^{+}} \left[I_{\rho} + \frac{c_{\rho}^{+} - c_{\rho}^{-}}{c_{\rho}^{-} + c_{\rho}^{+}} I_{\rho} \right] - \frac{h^{-}}{h+h^{-}} \frac{2c_{\rho}^{+}}{c_{\rho}^{-} + c_{\rho}^{+}} I_{\rho} + R_u^{+} ,$$

i.e.

$$T_u^{-} = I_{\rho} \frac{2c_{\rho}^{+}}{c_{\rho}^{-} + c_{\rho}^{+}} \left(\frac{h^{+}}{h+h^{+}} - \frac{h^{-}}{h+h^{-}} \right) + R_u^{+} . \quad (3.12)$$

Inclusion of term (3.12) in equation (3.10d) gives equation for R_u^{+} :

$$R_u^+ \left[\frac{h^- G^-}{h c_u^-} + \frac{h^+ G^+}{h c_u^+} \right] = 2I_\rho \left[g \frac{c_\rho^+ - c_\rho^-}{c_\rho^- c_\rho^+} - \frac{h^- G^-}{h c_u^-} \frac{c_\rho^+}{c_\rho^- + c_\rho^+} \left(\frac{h^+}{h+h^+} - \frac{h^-}{h+h^-} \right) \right].$$

By using terms for c_ρ^- , c_ρ^+ , c_u^- , c_u^+ , G^- and G^+ , the solution for R_u^+ is obtained, i.e. the amplitude of transmitted baroclinic wave in dependence on depths in the shallow and deep region, thermocline depth and stratification of water column (ε enters into equation through wave speed in the bottom layer and via terms G^- and G^+):

$$R_u^+ \left[\frac{h^- g \varepsilon \frac{h}{h+h^-}}{h \sqrt{g \varepsilon \frac{h h^-}{h+h^-}}} + \frac{h^+ g \varepsilon \frac{h}{h+h^+}}{h \sqrt{g \varepsilon \frac{h h^+}{h+h^+}}} \right] = 2I_\rho \left[g \frac{\sqrt{g(h+h^+)} - \sqrt{g(h+h^-)}}{\sqrt{g(h+h^-)} \sqrt{g(h+h^+)}} - \frac{h^-}{h} \frac{g \varepsilon \frac{h}{h+h^-}}{\sqrt{g \varepsilon \frac{h h^-}{h+h^-}}} \frac{\sqrt{g(h+h^+)}}{\sqrt{g(h+h^-)} + \sqrt{g(h+h^+)}} \left(\frac{h^+}{h+h^+} - \frac{h^-}{h+h^-} \right) \right].$$

Simplifying this and by changing $h^+ - h^- = H^+ - H^-$ one gets:

$$R_u^+ \left[\frac{\sqrt{h^- H^+} + \sqrt{h^+ H^-}}{\sqrt{H^-} \sqrt{H^+}} \right] = 2I_\rho \frac{\sqrt{H^+} - \sqrt{H^-}}{\sqrt{H^-} \sqrt{H^+}} \left[\frac{h}{\varepsilon} - \frac{h \sqrt{h^-}}{H^-} \right],$$

so that the final expression for R_u^+ is:

$$R_u^+ = 2I_\rho \frac{\sqrt{h}(\sqrt{H^+} - \sqrt{H^-})}{\sqrt{h^- H^+} + \sqrt{h^+ H^-}} \left[\frac{1}{\sqrt{\varepsilon}} - \frac{\sqrt{h h^-}}{H^-} \right]. \quad (3.13)$$

Finally, by using (3.13) in (3.12), the solution for T_u^- is:

$$T_u^- = 2I_\rho (\sqrt{H^+} - \sqrt{H^-}) \left[\frac{h}{H^- \sqrt{H^+}} + \frac{\sqrt{h}}{\sqrt{h^- H^+} + \sqrt{h^+ H^-}} \left(\frac{1}{\sqrt{\varepsilon}} - \frac{\sqrt{h h^-}}{H^-} \right) \right]. \quad (3.14)$$

In this way, the final solutions for equation (3.10) are found:

$$\begin{aligned}
R_p^+ &= I_p \frac{\sqrt{H^+} - \sqrt{H^-}}{\sqrt{H^-} + \sqrt{H^+}} \\
T_p^- &= I_p \frac{2\sqrt{H^+}}{\sqrt{H^-} + \sqrt{H^+}} \\
R_u^+ &= 2I_p \frac{\sqrt{h}(\sqrt{H^+} - \sqrt{H^-})}{\sqrt{h^-}H^+ + \sqrt{h^+}H^-} \left[\frac{1}{\sqrt{\varepsilon}} - \frac{\sqrt{hh^-}}{H^-} \right] \\
T_u^- &= 2I_p (\sqrt{H^+} - \sqrt{H^-}) \left[\frac{h}{H^- \sqrt{H^+}} + \frac{\sqrt{h}}{\sqrt{h^-}H^+ + \sqrt{h^+}H^-} \left(\frac{1}{\sqrt{\varepsilon}} - \frac{\sqrt{hh^-}}{H^-} \right) \right].
\end{aligned} \tag{3.15}$$

The main factor contributing to the amplification of tidal signal on thermocline (pycnocline) because of the depth change is:

$$2I_p \frac{\sqrt{h}(\sqrt{H^+} - \sqrt{H^-})}{\sqrt{h^-}H^+ + \sqrt{h^+}H^-} \frac{1}{\sqrt{\varepsilon}},$$

which shows that thermocline oscillations are more pronounced if thermocline depth is larger, if density difference between the surface and bottom layer is smaller, and if amplitude of incoming surface tidal wave is larger. When shallow region depth is increased, intensification decreases, while an increase of deep region depth gives more significant amplification (Figure 15). These results are in accordance with previous analysis for two-layer analytical models (e.g. *Ratray*, 1960).

Surface and interface elevations can be found from expressions connecting solutions for the surface and internal mode (equations are valid both in the shallow and deep regions of the model, so they are quoted in original notation):

$$\begin{aligned}
\zeta &= \zeta_p + \zeta_u = \zeta_p \\
\zeta' &= \zeta'_p + \zeta'_u = \frac{h'}{h+h'} \zeta_p + \zeta'_u,
\end{aligned}$$

so that in the shallow region (−) and deep region (+), which are now being denoted by (1) and (2), sea surface elevation and thermocline elevation are given by:

$$(\zeta)_1 = \zeta_p^- = T_p^- \exp[i(\omega t + k_p^- x)]$$

$$(\zeta')_1 = \frac{h^-}{h+h^-} \zeta_p^- + \zeta_u^- = \frac{h^-}{h+h^-} T_p^- \exp[i(\omega t + k_p^- x)] + T_u^- \exp[i(\omega t + k_u^- x)]$$

$$(\zeta)_2 = \zeta_p^+ = I_p^+ \exp[i(\omega t + k_p^+ x)] + R_p^+ \exp[i(\omega t - k_p^+ x)]$$

$$(\zeta')_2 = \frac{h^+}{h+h^+} \zeta_p^+ + \zeta_u^+ = \frac{h^+}{h+h^+} \{I_p^+ \exp[i(\omega t + k_p^+ x)] + R_p^+ \exp[i(\omega t - k_p^+ x)]\} + R_u^+ \exp[i(\omega t - k_u^+ x)].$$

The distribution of the ratio between thermocline elevation (ζ') and sea surface elevation (ζ) is given in Figure 15, for $x=0$ and range of depths of the shallow and deep region. In this example thermocline depth was set to $h=25$ m, while stratification coefficient was taken to be $\varepsilon = 0.00045$. These parameters correspond to the characteristics of stratification in June 2001, when strong diurnal tidal oscillations were detected at Lastovo, in the layer between 15 and 36 m (Mihanovic, 2005). Thermocline oscillations were significantly correlated with the surface tidal signal at Dubrovnik. The deeper the shallow region, the smaller the ratio between thermocline elevation and surface elevation, the deeper the deep region, the larger the ratio.

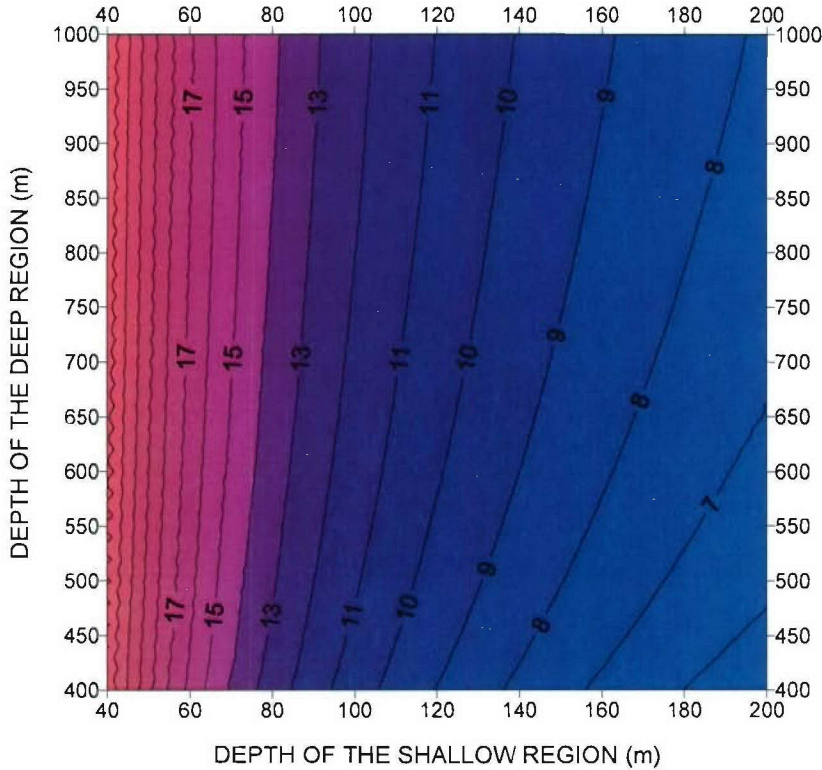


Figure 15. The distribution of the ratio between thermocline elevation and sea surface elevation for $x=0$ and assumed thermocline depth $h=25$ m, with stratification coefficient $\varepsilon = 0.00045$.

The distribution of the ratio between thermocline elevation and sea surface elevation, at $x = 0$, for different values of thermocline depth and stratification coefficient, can be seen in Figure 16. South Adriatic shelf profile between Lastovo island and the middle part of the South Adriatic Pit was analyzed. The least squares method gives the depth of shallow region $H^- = 150$ m, and the depth of deep region $H^+ = 1170$ m. The influence of thermocline depth increase and stratification reduction on thermocline oscillations amplification is evident. When parameters measured in June 2001 are taken into account (red lines in Figure 16), analytical model with progressive wave propagating from deep into shallow region gives the ratio of thermocline oscillations and sea surface oscillations of about 10. The data from June 2001 demonstrate that the ratios of maximum filtered values range between 9 and 39 (the envelope of surface elevation has smaller amplitude than thermocline elevation envelope). If only monthly maxima are taken into consideration, the ratio is about 29. Harmonic analysis of K1 tidal components showed that the amplitude ratio was approximately 21 (Mihanovic, 2005).

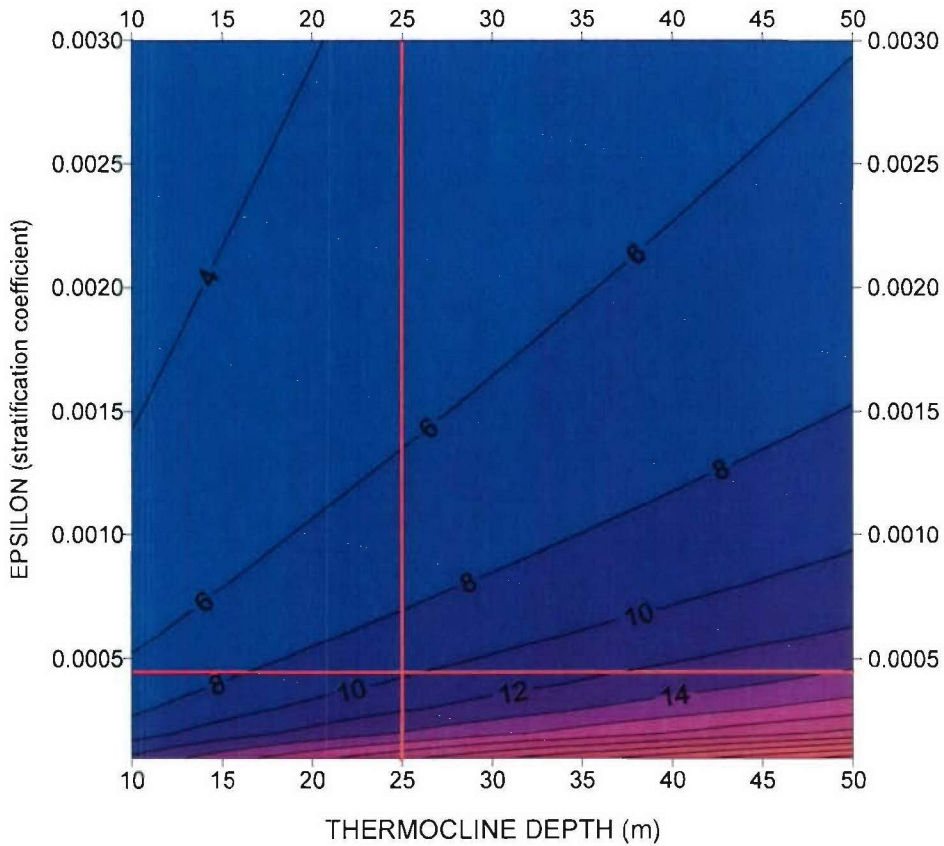


Figure 16. The distribution of the ratio between thermocline elevation and sea surface elevation for $x = 0$ and assumed shallow region depth $H^- = 150$ m and deep region depth $H^+ = 1170$ m (profile Lastovo – South Adriatic Pit). Red lines denote thermocline depth ($h = 25$ m) and stratification ($\varepsilon = 0.00045$) as measured in June 2001 (Mihanovic, 2005).

These results imply that the model defined in this way can reproduce relationship between thermocline elevation and surface elevation, despite the model limitations (two-layer analytical model, abrupt topography change at the shelf break). However, in progressive wave consideration, surface oscillations and current oscillations are in phase, which does not comply with K1 tidal component characteristics in the Adriatic. Measurements from July 1990 and August 1991 showed that this relationship is closer to standing surface wave character, since current oscillations precede surface oscillations by about 90° (Mihanovic, 2005). Therefore, the model results with the standing surface wave will be considered in the next section.

3. 3. Standing surface wave

Harmonic analysis of sea currents in a wider Lastovo area showed that maxima of barotropic flow precede maxima of sea level by about 90° . Analytical model with progressive surface wave cannot reproduce this phase relationship, since for progressive wave the flow and sea level oscillations are in phase. Consequently, two-layer analytical model with assumption of a standing surface wave was also developed. As in previous section, elevation continuity condition in the surface and bottom layer, as well as flow continuity in the entire water column and separately in the surface and bottom layer, needs to be fulfilled.

Generally, system of equations for the surface (3.4) and internal mode (3.5) can be written in transformed form, which uses surface mode flow and internal mode flow in the surface layer, instead of speed of the surface and internal mode. The notation is original, i.e. h is depth of the surface layer, h' is depth of the bottom layer, u and ζ represent speed and elevation of the surface layer, while u' and ζ' represent speed and elevation of the bottom layer. If speed and elevation of the surface mode are denoted by \tilde{u}_p and $\tilde{\zeta}_p$, and speed and elevation of the internal mode by \tilde{u}_u and $\tilde{\zeta}_u$, new variables can be defined, which will be used in transformed system of equations. These new variables are as follows:

- $U_p = (h + h')\tilde{u}_p$ - surface mode flow,
- $\zeta_p = \tilde{\zeta}_p$ - surface mode elevation (equals surface elevation),
- $U_u = h\tilde{u}_u$ - internal mode flow in the surface layer, and
- $\zeta_u = -\tilde{\zeta}_u$ - transformed internal mode elevation (enables similar equations for both modes).

Equations for the surface and internal mode now become:

$$\begin{aligned}
 & \frac{\partial U_p}{\partial t} + c_p^2 \frac{\partial \zeta_p}{\partial x} = 0 \\
 \text{surface mode:} & \qquad \qquad \qquad \text{where } c_p^2 = g(h + h'), \qquad (3.16) \\
 & \frac{\partial \zeta_p}{\partial t} + \frac{\partial U_p}{\partial x} = 0
 \end{aligned}$$

$$\begin{aligned}
& \frac{\partial U_u}{\partial t} + c_u^2 \frac{\partial \zeta_u}{\partial x} = 0 \\
\text{internal mode:} & \quad \text{where } c_u^2 = g\varepsilon \frac{hh'}{h+h'}. \quad (3.17) \\
& \frac{\partial \zeta_u}{\partial t} + \frac{\partial U_u}{\partial x} = 0
\end{aligned}$$

Boundary conditions at depth discontinuity are equal elevations and flows at $x = 0$, giving:

$$\text{surface mode:} \quad U_p \text{ and } \zeta_p \text{ are preserved at depth discontinuity,} \quad (3.18a)$$

$$\begin{aligned}
& -\zeta_u + \frac{h'}{h+h'} \zeta_p \text{ is preserved at depth discontinuity,} \\
\text{internal mode:} & \quad (3.18b)
\end{aligned}$$

$$\frac{h}{h+h'} U_p + U_u \text{ is preserved at depth discontinuity.}$$

The relationship with the original variables (speed and elevation of the surface layer, and speed and elevation of the bottom layer) is defined by:

$$u = \frac{1}{h+h'} U_p + \frac{1}{h} U_u \quad (3.19a)$$

$$\zeta = \zeta_p \quad (3.19b)$$

$$u' = \frac{1}{h+h'} U_p - \frac{1}{h'} U_u \quad (3.19c)$$

$$\zeta' = \frac{h'}{h+h'} \zeta_p - \zeta_u. \quad (3.19d)$$

In the following equations, all variables to the left of the origin (depth discontinuity) will be denoted by “-”, and those to the right by “+”, so that the apostrophe mark is temporarily lost. Therefore, depths of the bottom layer on the left and on the right side of topography jump become, as in section 3.2, h^- and h^+ . Additional abbreviation is introduced:

$$b = \frac{h(h^+ - h^-)}{(h+h^+)(h+h^-)}.$$

Generally, the solution will be:

$$X(x,t) = \begin{bmatrix} U_p(x,t) \\ \zeta_p(x,t) \\ U_u(x,t) \\ \zeta_u(x,t) \end{bmatrix} = X(x)e^{i\omega x} = \begin{bmatrix} U_p(x) \\ \zeta_p(x) \\ U_u(x) \\ \zeta_u(x) \end{bmatrix} \cdot e^{i\omega x},$$

meaning that the solution has a defined angular frequency ω . The solutions of equations (3.16) and (3.17) can be written separately for the left and right side. For the left side:

$$X^-(x) = \begin{bmatrix} U_p^-(x) \\ \zeta_p^-(x) \\ U_u^-(x) \\ \zeta_u^-(x) \end{bmatrix} = \begin{bmatrix} \cos \frac{\omega}{c_p^-} x & -ic_p^- \sin \frac{\omega}{c_p^-} x & 0 & 0 \\ -\frac{i}{c_p^-} \sin \frac{\omega}{c_p^-} x & \cos \frac{\omega}{c_p^-} x & 0 & 0 \\ -\frac{b}{2} \cos \frac{\omega}{c_u^-} x & \frac{ib}{2} c_u^- \sin \frac{\omega}{c_u^-} x & \cos \frac{\omega}{c_u^-} x & -ic_u^- \sin \frac{\omega}{c_u^-} x \\ \frac{ib}{2c_u^-} \sin \frac{\omega}{c_u^-} x & -\frac{b}{2} \cos \frac{\omega}{c_u^-} x & -\frac{i}{c_u^-} \sin \frac{\omega}{c_u^-} x & \cos \frac{\omega}{c_u^-} x \end{bmatrix} \begin{bmatrix} U_p(0) \\ \zeta_p(0) \\ U_u^{(sr)}(0) \\ \zeta_u^{(sr)}(0) \end{bmatrix}, \quad (3.20)$$

where $U_p(0)$, $\zeta_p(0)$ represent values of flow and elevation of the surface mode at $x=0$ (preserved on depth discontinuity), while $U_u^{(sr)}(0)$, $\zeta_u^{(sr)}(0)$ represent average values of corresponding parameters for the internal mode on both sides of discontinuity (not preserved). These four complex numbers completely determine the solution of the form $X(x)e^{i\omega x}$.

For the right side the solution is:

$$X^+(x) = \begin{bmatrix} U_p^+(x) \\ \zeta_p^+(x) \\ U_u^+(x) \\ \zeta_u^+(x) \end{bmatrix} = \begin{bmatrix} \cos \frac{\omega}{c_p^+} x & -ic_p^+ \sin \frac{\omega}{c_p^+} x & 0 & 0 \\ -\frac{i}{c_p^+} \sin \frac{\omega}{c_p^+} x & \cos \frac{\omega}{c_p^+} x & 0 & 0 \\ \frac{b}{2} \cos \frac{\omega}{c_u^+} x & -\frac{ib}{2} c_u^+ \sin \frac{\omega}{c_u^+} x & \cos \frac{\omega}{c_u^+} x & -ic_u^+ \sin \frac{\omega}{c_u^+} x \\ -\frac{ib}{2c_u^+} \sin \frac{\omega}{c_u^+} x & \frac{b}{2} \cos \frac{\omega}{c_u^+} x & -\frac{i}{c_u^+} \sin \frac{\omega}{c_u^+} x & \cos \frac{\omega}{c_u^+} x \end{bmatrix} \begin{bmatrix} U_p(0) \\ \zeta_p(0) \\ U_u^{(sr)}(0) \\ \zeta_u^{(sr)}(0) \end{bmatrix}. \quad (3.21)$$

This solution is proportional to $e^{i\omega x}$, i.e. it is related to frequency ω . Frequency $-\omega$ has complex conjugate solution, i.e. \bar{X}^- and \bar{X}^+ . Therefore, respective constants $U_p(0)$, ..., $\zeta_u^{(sr)}(0)$ form complex conjugate pairs and by combining both solutions

one can find real solution characterized by frequency ω . Thermocline elevation (3.19d) contains reduced surface mode elevation and internal mode elevation, which include four terms in the last row of (3.20) and (3.21). The amplification of thermocline elevation arises from terms which multiply $U_p(0)$ and $\zeta_u^{(sr)}(0)$. It is obvious that term connected with $U_p(0)$ is divided by the speed of internal waves c_u^\pm , which is significantly smaller than the speed of surface waves, contributing to amplification on thermocline. Intensification related to $\zeta_u^{(sr)}(0)$ is not seen directly, because it comes from the constant already having amplified thermocline elevation. It becomes more comprehensible when boundary conditions at the ends of the basin are included, thus enabling the boundary problem to be solved. On the other hand, this term is essential for reproducing propagating character of internal waves. Therefore, two different cases of solution with boundary conditions taken into account will be presented in this report. First, the problem will be solved with classical boundary conditions on the left and right end of the basin for the surface and internal mode (at the closed boundary no normal flow condition, and at the open boundary zero elevation condition). After that, the analysis of a problem in which surface mode is subjected to classical boundary conditions and internal mode to radiation boundary condition will be offered (so that the boundaries of the basin do not affect wave disturbance, allowing complete energy transmission). Schematic presentation of a basin that will represent the Adriatic is given in Figure 17. The left end of the basin at $x = L_1 < 0$ is closed, whilst the right end at $x = L_2 > 0$ is open, i.e. it borders with an ocean of infinite depth.

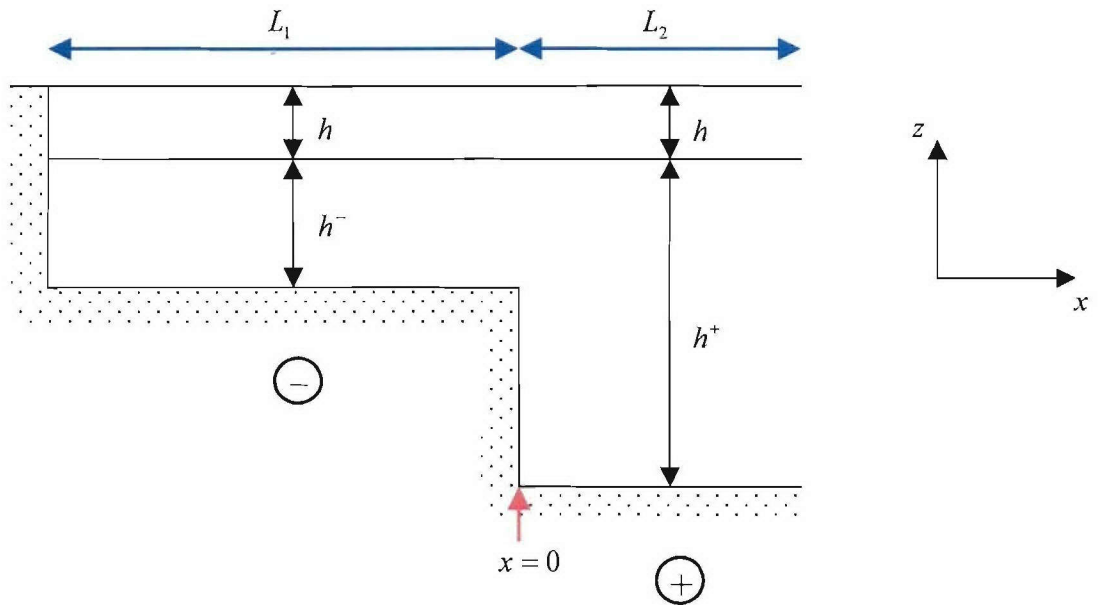


Figure 17. Schematic presentation of an idealized topography for two-layer analytical model with shelf region (-) and deep sea region (+). In the shelf region (-) the basin is closed, and in the deep sea region (+) it borders with an ocean of infinite depth.

In order to implement the analytical model to the Adriatic, it is necessary to determine parameters that approximate the Adriatic Sea with a two-dimensional basin closed at left end, and opened at the right end, with rapid depth change at the shelf break.

Parameters which are included in the model are depths of the shallow and deep region (H^- and H^+), together with distance of the closed (L_1) and open end (L_2) from the origin. These parameters were resolved in three ways. The first approximation that was used is the Adriatic transversal cross section approximation, with sections that are 20.5 km apart (Sterneck, 1919), which enabled calculation of average depths of these sections along the Adriatic. Next, these values separated by 20.5 km were interpolated every 0.5 km enabling more precise discretization and better resolving of depth discontinuity position. The third Adriatic approximation is based on longitudinal cross section along central Adriatic line, also interpolated every 0.5 km.

Three different parameterizations of the Adriatic are shown in Figure 18:

- parameterization according to Sterneck, spacing equals 20.5 km,
- parameterization according to Sterneck, spacing equals 0.5 km,
- central longitudinal Adriatic cross section, spacing equals 0.5 km.

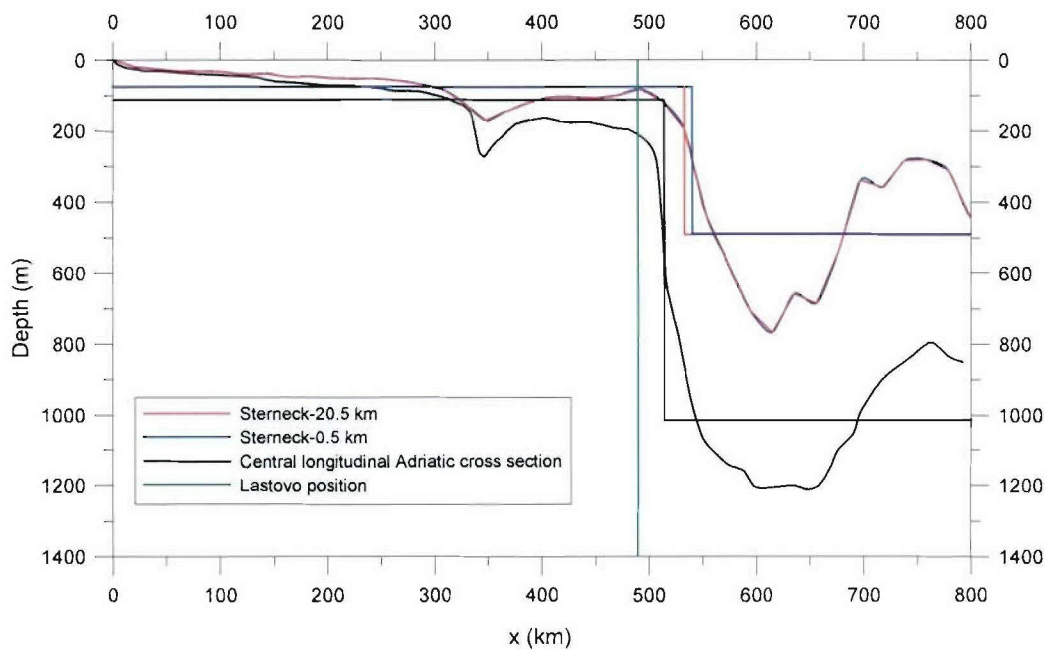


Figure 18. The Adriatic Sea approximated by a two-dimensional basin with three different parameterizations. Green line denotes geographical position of Lastovo in idealized basin representing the Adriatic.

The exact position of the depth discontinuity, together with depths of the shallow and deep region, was resolved by applying the least squares method on depth values distributed along the Adriatic. Lastovo island is located around 490 km from the closed end of the basin (represented by green line in Figure 18). Once the coordinate of the discontinuity is determined, origin is positioned at this coordinate, and model parameters are defined. They are given in Table 2, for each parameterization in respective coordinate system. Depths are smaller for Sterneck's approximations because they comprise average depth of each transversal transect, whereas

longitudinal Adriatic cross section includes maximum depths on transversal cross sections.

In the three cases we have used thermocline depth and stratification coefficient as calculated for June 2001 and Lastovo ($h = 25$ m, $\varepsilon = 0.00045$, *Mihanovic, 2005*).

Table 2. Parameters required for the two-dimensional analytical model including a standing surface wave and three different approximations of the Adriatic.

	Sterneck 20.5 km	Sterneck 0.5 km	Central longitudinal cross section of the Adriatic
L_1	-533 km	-540.5 km	-514 km
L_2	267 km	259.5 km	286 km
H^-	76.5 m	77.6 m	111.9 m
H^+	491.7 m	489.9 m	1014.5 m
Lastovo	-43 km	-50.5 km	-24 km

3. 3. 1. Classical boundary conditions at the closed and open end of the basin for the surface and internal mode

Classical boundary conditions for the surface and internal mode are basic assumptions of the model, from which relationship between constants $U_p(0)$, ..., $\zeta_u^{(sr)}(0)$ can be found, i.e. connection between surface oscillations and thermocline response may be determined. At the closed end of the basin, corresponding flows are zero, as are elevations at the open end:

$$\text{closed (left) end of the basin: } U_p(L_1) = 0, \quad U_u(L_1) = 0, \quad (3.22a)$$

$$\text{open (right) end of the basin: } \zeta_p(L_2) = 0, \quad \zeta_u(L_2) = 0. \quad (3.22b)$$

It is necessary to resolve the frequency ω , together with constants $U_p(0)$, $\zeta_p(0)$, $U_u^{(sr)}(0)$ and $\zeta_u^{(sr)}(0)$, so that solutions (3.20) and (3.21) comply with boundary conditions (3.22). In the following equations these constants will be denoted by y_1 , y_2 , y_3 and y_4 . Non-trivial solutions of system (3.23) need to be found:

$$\begin{bmatrix} \cos \frac{\omega L_1}{c_p^-} & -ic_p^- \sin \frac{\omega L_1}{c_p^-} & 0 & 0 \\ -\frac{i}{c_p^+} \sin \frac{\omega L_2}{c_p^+} & \cos \frac{\omega L_2}{c_p^+} & 0 & 0 \\ -\frac{b}{2} \cos \frac{\omega L_1}{c_u^-} & \frac{ib}{2} c_u^- \sin \frac{\omega L_1}{c_u^-} & \cos \frac{\omega L_1}{c_u^-} & -ic_u^- \sin \frac{\omega L_1}{c_u^-} \\ -\frac{ib}{2c_u^+} \sin \frac{\omega L_2}{c_u^+} & \frac{b}{2} \cos \frac{\omega L_2}{c_u^+} & -\frac{i}{c_u^+} \sin \frac{\omega L_2}{c_u^+} & \cos \frac{\omega L_2}{c_u^+} \end{bmatrix} \begin{bmatrix} y_1 \\ y_2 \\ y_3 \\ y_4 \end{bmatrix} = \begin{bmatrix} 0 \\ 0 \\ 0 \\ 0 \end{bmatrix}. \quad (3.23)$$

Non-trivial solutions exist for those ω for which determinant of the system is zero, i.e.:

$$\left(\cos \frac{\omega L_1}{c_p^-} \cos \frac{\omega L_2}{c_p^+} + \frac{c_p^-}{c_p^+} \sin \frac{\omega L_1}{c_p^-} \sin \frac{\omega L_2}{c_p^+} \right) \left(\cos \frac{\omega L_1}{c_u^-} \cos \frac{\omega L_2}{c_u^+} + \frac{c_u^-}{c_u^+} \sin \frac{\omega L_1}{c_u^-} \sin \frac{\omega L_2}{c_u^+} \right) = 0. \quad (3.24)$$

If the term in the first bracket equals zero, natural frequencies of *surface modes* are found, whereas the second bracket equaling zero gives *internal modes* frequencies. Natural frequencies of surface modes essentially represent characteristic frequencies of fundamental mode and higher seiche modes for basin defined by depths and distances from the closed and open basin boundary. For these frequencies, one needs to solve system (3.23). For internal modes $y_1 = y_2 = 0$, so that they are manifested only through ζ_u and U_u . For surface modes, all four parameters are non-zero, meaning that surface modes influence all four variables, i.e. surface and internal elevation and speed. It is important to emphasize that y_3 and y_4 depend on y_1 and y_2 in a way which depends on given boundary conditions.

If the lower right 2×2 matrix in (3.23) is denoted by D_u , i.e.

$$D_u = \begin{bmatrix} \cos \frac{\omega L_1}{c_u^-} & -ic_u^- \sin \frac{\omega L_1}{c_u^-} \\ -\frac{i}{c_u^+} \sin \frac{\omega L_2}{c_u^+} & \cos \frac{\omega L_2}{c_u^+} \end{bmatrix},$$

the relationship between y_3 and y_4 as well as y_1 and y_2 could be expressed as:

$$\begin{bmatrix} y_3 \\ y_4 \end{bmatrix} = -\frac{b}{2} D_u^{-1} \begin{bmatrix} -1 & 0 \\ 0 & 1 \end{bmatrix} D_u \begin{bmatrix} y_1 \\ y_2 \end{bmatrix},$$

or:

$$\begin{bmatrix} y_3 \\ y_4 \end{bmatrix} = \frac{b}{2 \det(D_u)} \cdot \begin{bmatrix} \cos \frac{\omega L_1}{c_u^-} \cos \frac{\omega L_2}{c_u^+} - \frac{c_u^-}{c_u^+} \sin \frac{\omega L_1}{c_u^-} \sin \frac{\omega L_2}{c_u^+} & -2ic_u^- \sin \frac{\omega L_1}{c_u^-} \cos \frac{\omega L_2}{c_u^+} \\ \frac{2i}{c_u^+} \cos \frac{\omega L_1}{c_u^-} \sin \frac{\omega L_2}{c_u^+} & \frac{c_u^-}{c_u^+} \sin \frac{\omega L_1}{c_u^-} \sin \frac{\omega L_2}{c_u^+} - \cos \frac{\omega L_1}{c_u^-} \cos \frac{\omega L_2}{c_u^+} \end{bmatrix} \begin{bmatrix} y_1 \\ y_2 \end{bmatrix}. \quad (3.25)$$

Also, from equation (3.23), for ω which cancels out the left bracket in (3.24), one can get:

$$\begin{bmatrix} y_1 \\ y_2 \end{bmatrix} = \begin{bmatrix} ic_p^- \sin \frac{\omega L_1}{c_p^-} \\ \cos \frac{\omega L_1}{c_p^-} \end{bmatrix},$$

which together with previous equation gives:

$$\begin{bmatrix} y_3 \\ y_4 \end{bmatrix} = \frac{b}{2 \det(D_u)} \cdot \begin{bmatrix} ic_p^- \sin \frac{\omega L_1}{c_p^-} \left(\cos \frac{\omega L_1}{c_u^-} \cos \frac{\omega L_2}{c_u^+} - \frac{c_u^-}{c_u^+} \sin \frac{\omega L_1}{c_u^-} \sin \frac{\omega L_2}{c_u^+} \right) & -2ic_u^- \sin \frac{\omega L_1}{c_u^-} \cos \frac{\omega L_2}{c_u^+} \cos \frac{\omega L_1}{c_p^-} \\ -2 \frac{c_p^-}{c_u^+} \cos \frac{\omega L_1}{c_u^-} \sin \frac{\omega L_2}{c_u^+} \sin \frac{\omega L_1}{c_p^-} & \left(\frac{c_u^-}{c_u^+} \sin \frac{\omega L_1}{c_u^-} \sin \frac{\omega L_2}{c_u^+} - \cos \frac{\omega L_1}{c_u^-} \cos \frac{\omega L_2}{c_u^+} \right) \cos \frac{\omega L_1}{c_p^-} \end{bmatrix}.$$

By substituting solutions y_1 , y_2 , y_3 and y_4 with $U_p(0)$, $\zeta_p(0)$, $U_u^{(sr)}(0)$ and $\zeta_u^{(sr)}(0)$ in (3.20), the solution for the left side of the basin in matrix form is found (the solution for the right side is analogous, according to (3.21)):

$$\begin{bmatrix} U_p^-(x) \\ \zeta_p^-(x) \\ U_u^-(x) \\ \zeta_u^-(x) \end{bmatrix} = \begin{bmatrix} \cos \frac{\omega}{c_p^-} x \cdot y_1 - i c_p^- \sin \frac{\omega}{c_p^-} x \cdot y_2 \\ -\frac{i}{c_p^-} \sin \frac{\omega}{c_p^-} x \cdot y_1 + \cos \frac{\omega}{c_p^-} x \cdot y_2 \\ -\frac{b}{2} \cos \frac{\omega}{c_u^-} x \cdot y_1 + \frac{ib}{2} c_u^- \sin \frac{\omega}{c_u^-} x \cdot y_2 + \cos \frac{\omega}{c_u^-} x \cdot y_3 - i c_u^- \sin \frac{\omega}{c_u^-} x \cdot y_4 \\ \frac{ib}{2c_u^-} \sin \frac{\omega}{c_u^-} x \cdot y_1 - \frac{b}{2} \cos \frac{\omega}{c_u^-} x \cdot y_2 - \frac{i}{c_u^-} \sin \frac{\omega}{c_u^-} x \cdot y_3 + \cos \frac{\omega}{c_u^-} x \cdot y_4 \end{bmatrix}. \quad (3.26)$$

By arranging elevation terms on the left side and on the right side of the origin, final solutions that enable comparison of oscillations in the surface and bottom layer are obtained:

$$\zeta_p^- = \cos \left[\frac{\omega}{c_p^-} (x - L_1) \right] \quad (3.27a)$$

$$\zeta_u^- = -\frac{b}{\det(D_u)} \left[\frac{c_p^-}{c_u^+} \sin \frac{\omega L_1}{c_p^-} \sin \frac{\omega L_2}{c_u^+} + \cos \frac{\omega L_1}{c_p^-} \cos \frac{\omega L_2}{c_u^+} \right] \cdot \cos \left[\frac{\omega}{c_u^-} (x - L_1) \right] \quad (3.27b)$$

$$\zeta_p^+ = -\frac{\cos \frac{\omega L_1}{c_p^-}}{\sin \frac{\omega L_2}{c_p^+}} \cdot \sin \left[\frac{\omega}{c_p^+} (x - L_2) \right] \quad (3.27c)$$

$$\zeta_u^+ = \frac{b}{\det(D_u)} \left[\frac{c_p^-}{c_u^+} \sin \frac{\omega L_1}{c_p^-} \cos \frac{\omega L_1}{c_u^-} - \frac{c_u^-}{c_u^+} \cos \frac{\omega L_1}{c_p^-} \sin \frac{\omega L_1}{c_u^-} \right] \cdot \sin \left[\frac{\omega}{c_u^+} (x - L_2) \right]. \quad (3.27d)$$

Surface layer elevation and bottom layer elevation are obtained from solutions for the surface and internal mode according to (3.19).

General solutions (3.20) and (3.21) demand designation of flow and elevation for the surface mode ($U_p(0)$, $\zeta_p(0)$), as well as average values of flow and elevation for the internal mode ($U_u^{(sr)}(0)$, $\zeta_u^{(sr)}(0)$) at depth discontinuity. If the average values for the internal mode are disregarded, i.e. if it is supposed:

$$\begin{bmatrix} U_p(0) \\ \zeta_p(0) \\ U_u^{(sr)}(0) \\ \zeta_u^{(sr)}(0) \end{bmatrix} \approx \begin{bmatrix} c_p \cdot A \\ A \\ 0 \\ 0 \end{bmatrix},$$

amplification for ζ_u is obtained only through the sine term (factor c_p/c_u multiplies sine in the lower left element of (3.20) and (3.21)). This ignores the influence of surface mode on internal mode, which emerges clearly when solving the boundary problem, where surface mode values (y_1 and y_2) determine values for internal mode (y_3 and y_4). This is explicitly clear in equation (3.25). Factor c_p/c_u is evident in the term for y_4 , and comes from y_1 (representing the speed at depth discontinuity). Hence, the speed at topography discontinuity in the internal mode is responsible for amplification of thermocline oscillations. Factor c_p/c_u in the final solution represents this intensification, and it can be seen in sine term (through y_1) and in cosine term (through y_4), which is in accordance with progressive character of internal waves.

The results of analytical model for the surface and bottom layer, with classical boundary conditions at the closed and open end of the basin, are given in Figures 19 – 21. Three parameterizations of the Adriatic were used, corresponding to a two-dimensional basin with a depth discontinuity (Figure 18 and Table 2). Geographical position of Lastovo island is marked by a green line. Since the solutions given in (3.27) are defined up to an arbitrary constant, results with the supposed surface amplitude of 1 m at the closed end of the basin are presented.

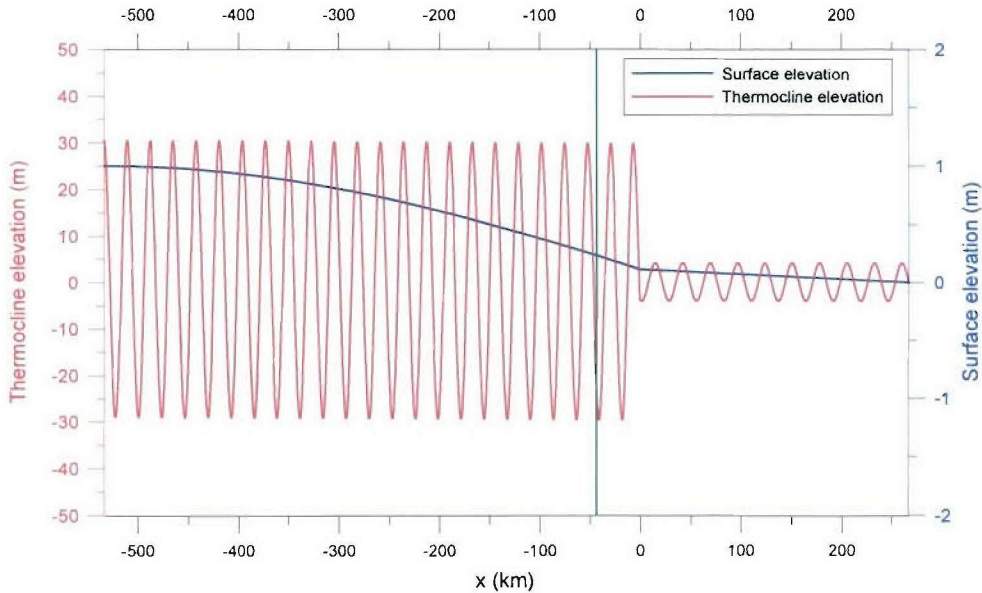


Figure 19. The results of the two-layer analytical model for the surface and bottom layer with classical boundary conditions at the closed and open end of the basin, and parameterization of the Adriatic according to Sterneck, with spacing of 20.5 km. The position of Lastovo is marked by a green line.

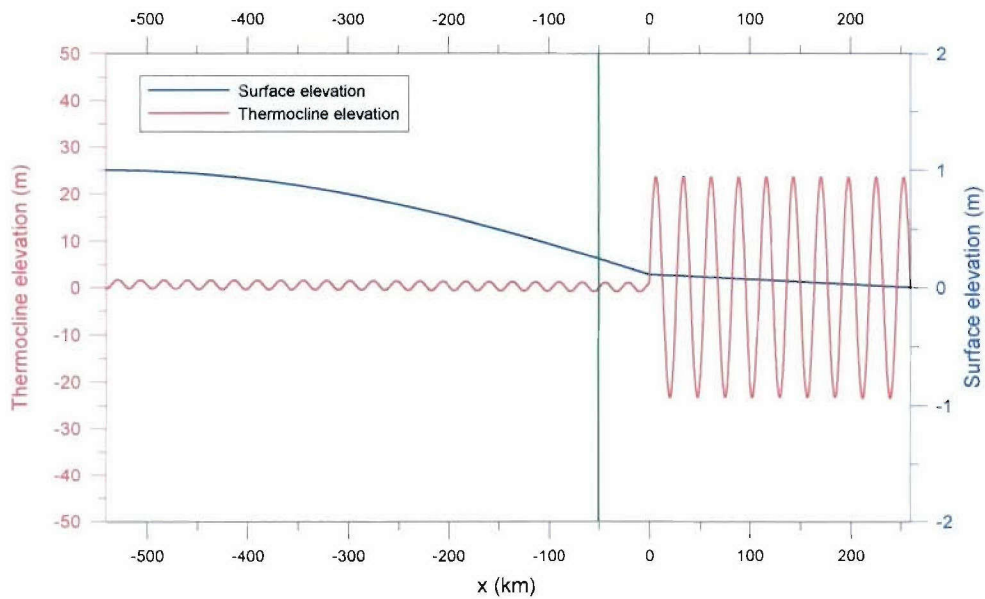


Figure 20. The results of the two-layer analytical model for the surface and bottom layer with classical boundary conditions at the closed and open end of the basin, and parameterization of the Adriatic according to Sterneck, with spacing of 0.5 km. The position of Lastovo is marked by a green line.

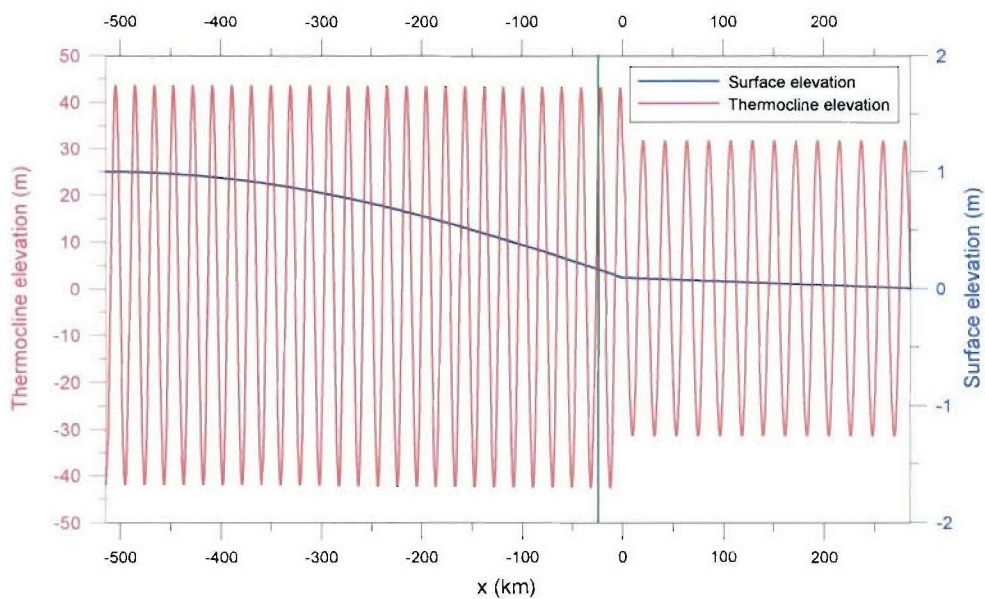


Figure 21. The results of the two-layer analytical model for the surface and bottom layer with classical boundary conditions at the closed and open end of the basin, and parameterization of the Adriatic along central longitudinal cross section, with spacing of 0.5 km. The position of Lastovo is marked by a green line.

By solving equations (3.24) natural frequencies of the surface modes are calculated. They represent characteristic frequencies of fundamental mode and higher seiche modes in the basin defined by depths of shallow and deep region, as well as by distances of closed and open boundary from the origin. Parameterization of the Adriatic according to Sterneck gives period of the fundamental mode of about 23.34 h (for spacing of 20.5 km) and 23.46 h (for spacing of 0.5 km). When central longitudinal Adriatic approximation is used, the fundamental mode period is about 18.32 h. These estimates are close to measured values of fundamental seiche period in the Adriatic, which lie between 21.4 and 22.4 h (*Buljan and Zore-Armanda, 1976; Mosetti and Purga, 1983*), taking into account that these are approximations of the Adriatic by a simple two-dimensional analytical model. Estimates calculated from Sterneck's parameterizations are closer to cited periods, since depth values represent average values at a transversal cross section. In the central longitudinal Adriatic cross section, only maximum depths are used, giving smaller fundamental mode period for this approximation.

All three parameterizations give amplification of thermocline oscillations with respect to surface oscillations. However, the ratio of amplitudes as well as phase relationship sensitively depend on selection of depth parameters (shallow and deep region) and of distances of the closed and open boundary from the origin. Since solutions for the surface and bottom layer are in the form of standing waves, and since lengths of internal waves are much smaller than those of surface waves, oscillations can be either in phase or opposed in phase. In the case of Sterneck's parameterization with spacing of 20.5 km (Figure 19), significant amplification is detected at Lastovo position (about 100 times). Yet, oscillations are opposed in phase, which is not in accordance with observed "in phase" relationship (*Mihanovic, 2005*). A slight change of parameters for Sterneck's 0.5 km parameterization gives completely different results (Figure 20). The amplification of oscillations is more pronounced in deep region of the basin, and Lastovo is positioned almost at the nodal point of internal standing waves. This results in insignificant thermocline oscillations at this location (the ratio between thermocline elevation amplitude and surface elevation amplitude is about 0.2). Finally, parameterization of the Adriatic based on central longitudinal cross section also gives significant amplification in both shallow and deep region, but again it shows sensitive dependence of the model on values of calculated parameters (Figure 21). More precisely, at Lastovo the thermocline and surface oscillations are in phase, and amplification ratio is about 190.

Considering that in the surface layer standing wave is presumed, and boundary conditions give maximum surface elevation at the closed boundary, surface oscillations have relatively small amplitude close to the origin (depth discontinuity) when compared with the oscillations near the closed boundary. For this reason, different basin parameterizations give unrealistic amplifications of thermocline oscillations. The ratios of thermocline and surface oscillations as well as phase differences between them depend on the bottom layer results and on the Lastovo position with respect to nodal points of internal standing waves. Therefore, it can be concluded that this analytical model explains to some extent physical origin of amplification of thermocline oscillations at depth discontinuity (velocity change, or better to say, barotropic flow change). However, it fails to reproduce phase and amplitude relationships as recorded in June 2001.

3. 3. 2. *Classical boundary conditions for the surface mode and radiation boundary condition for the internal mode at the closed and open end of the basin*

In previous section classical boundary conditions for the surface and internal mode were presumed. This section will deal with radiation boundary conditions for internal mode:

$$\text{closed (left) end of the basin: } U_p(L_1) = 0, \quad -\zeta_u(L_1) + \frac{h^-}{hc_u^-} U_u(L_1) = 0, \quad (3.28a)$$

$$\text{open (right) end of the basin: } \zeta_p(L_2) = 0, \quad -\zeta_u(L_2) - \frac{h^+}{hc_u^+} U_u(L_2) = 0. \quad (3.28b)$$

General solution of system of equations (3.16) and (3.17) can be written as:

$$X^-(x) = \begin{bmatrix} U_p^-(x) \\ \zeta_p^-(x) \\ U_u^-(x) \\ \zeta_u^-(x) \end{bmatrix} = \begin{bmatrix} \tilde{S}_p^-(x) & 0 \\ -\frac{b}{2} \tilde{S}_u^-(x) & \tilde{S}_u^-(x) \end{bmatrix} \begin{bmatrix} Y_p \\ Y_u \end{bmatrix}, \quad (3.29)$$

$$X^+(x) = \begin{bmatrix} U_p^+(x) \\ \zeta_p^+(x) \\ U_u^+(x) \\ \zeta_u^+(x) \end{bmatrix} = \begin{bmatrix} \tilde{S}_p^+(x) & 0 \\ \frac{b}{2} \tilde{S}_u^+(x) & \tilde{S}_u^+(x) \end{bmatrix} \begin{bmatrix} Y_p \\ Y_u \end{bmatrix}, \quad (3.30)$$

where following matrices were introduced:

$$\tilde{S}_p^- = \begin{bmatrix} \cos \frac{\omega}{c_p^-} x & -ic_p^- \sin \frac{\omega}{c_p^-} x \\ -\frac{i}{c_p^-} \sin \frac{\omega}{c_p^-} x & \cos \frac{\omega}{c_p^-} x \end{bmatrix}, \quad \tilde{S}_p^+ = \begin{bmatrix} \cos \frac{\omega}{c_p^+} x & -ic_p^+ \sin \frac{\omega}{c_p^+} x \\ -\frac{i}{c_p^+} \sin \frac{\omega}{c_p^+} x & \cos \frac{\omega}{c_p^+} x \end{bmatrix},$$

$$\tilde{S}_u^- = \begin{bmatrix} \cos \frac{\omega}{c_u^-} x & -ic_u^- \sin \frac{\omega}{c_u^-} x \\ -\frac{i}{c_u^-} \sin \frac{\omega}{c_u^-} x & \cos \frac{\omega}{c_u^-} x \end{bmatrix}, \quad \tilde{S}_u^+ = \begin{bmatrix} \cos \frac{\omega}{c_u^+} x & -ic_u^+ \sin \frac{\omega}{c_u^+} x \\ -\frac{i}{c_u^+} \sin \frac{\omega}{c_u^+} x & \cos \frac{\omega}{c_u^+} x \end{bmatrix},$$

and

$$Y_p = \begin{bmatrix} U_p(0) \\ \zeta_p(0) \end{bmatrix} = \begin{bmatrix} y_1 \\ y_2 \end{bmatrix}, \quad Y_u = \begin{bmatrix} U_u^{(sr)}(0) \\ \zeta_u^{(sr)}(0) \end{bmatrix} = \begin{bmatrix} y_3 \\ y_4 \end{bmatrix}.$$

Unknown coefficients y_1 , y_2 , y_3 and y_4 can be obtained by applying boundary conditions, which leads to the system of equations analogous to system (3.23):

$$\begin{bmatrix} D_p & \begin{bmatrix} 0 & 0 \\ 0 & 0 \end{bmatrix} \\ \begin{bmatrix} -1 & 0 \\ 0 & 1 \end{bmatrix} D_u & D_u \end{bmatrix} \begin{bmatrix} Y_p \\ Y_u \end{bmatrix} = \begin{bmatrix} 0 \\ 0 \\ 0 \\ 0 \end{bmatrix}, \quad (3.31)$$

where following matrices were introduced:

$$D_p = \begin{bmatrix} \cos \frac{\omega L_1}{c_p^-} & -ic_p^- \sin \frac{\omega L_1}{c_p^-} \\ -\frac{i}{c_p^+} \sin \frac{\omega L_2}{c_p^+} & \cos \frac{\omega L_2}{c_p^+} \end{bmatrix},$$

$$D_u = \begin{bmatrix} \frac{i}{c_u^-} \sin \frac{\omega L_1}{c_u^-} + \frac{h^-}{hc_u^-} \cos \frac{\omega L_1}{c_u^-} & \cos \frac{\omega L_1}{c_u^-} + \frac{ih^-}{h} \sin \frac{\omega L_1}{c_u^-} \\ \frac{i}{c_u^+} \sin \frac{\omega L_2}{c_u^+} - \frac{h^+}{hc_u^+} \cos \frac{\omega L_2}{c_u^+} & \cos \frac{\omega L_2}{c_u^+} + \frac{ih^+}{h} \sin \frac{\omega L_2}{c_u^+} \end{bmatrix}.$$

Natural frequencies are solutions of the equation:

$$\det(D_p) \cdot \det(D_u) = 0, \quad (3.32)$$

where left factor corresponds to surface modes, the right one to internal modes. After obtaining frequency of the fundamental mode, from (3.23) it follows as before:

$$Y_p = \begin{bmatrix} ic_p^- \sin \frac{\omega L_1}{c_p^-} \\ \cos \frac{\omega L_1}{c_p^-} \end{bmatrix},$$

along with:

$$Y_u = D_u^{-1} \begin{bmatrix} -1 & 0 \\ 0 & 1 \end{bmatrix} D_u Y_p.$$

It is not necessary to explicitly calculate coefficients Y_u , because previous equation can be included into solutions (3.29) and (3.30):

$$X^-(x) = \begin{bmatrix} \tilde{S}_p^-(x) Y_p \\ \tilde{S}_u^-(x) \left(-\frac{b}{2} Y_p + Y_u \right) \end{bmatrix}, \quad X^+(x) = \begin{bmatrix} \tilde{S}_p^+(x) Y_p \\ \tilde{S}_u^+(x) \left(\frac{b}{2} Y_p + Y_u \right) \end{bmatrix}. \quad (3.33)$$

Finally, the terms which need to be written in complete form, introduced in (3.33), are:

$$-\frac{b}{2} Y_p + Y_u = -b D_u^{-1} \begin{bmatrix} 0 & 0 \\ 0 & 1 \end{bmatrix} D_u Y_p, \quad \frac{b}{2} Y_p + Y_u = b D_u^{-1} \begin{bmatrix} 1 & 0 \\ 0 & 0 \end{bmatrix} D_u Y_p. \quad (3.34)$$

The part of the solution corresponding to surface mode is the same as in previous section, while the solution for internal mode states:

$$\zeta_u^-(x) = \frac{-b \tilde{\zeta}_u^-(x)}{\det(D_u)}, \quad \zeta_u^+(x) = \frac{-b \tilde{\zeta}_u^+(x)}{\det(D_u)}, \quad (3.35)$$

$$U_u^-(x) = \frac{-b \tilde{U}_u^-(x)}{\det(D_u)}, \quad U_u^+(x) = \frac{-b \tilde{U}_u^+(x)}{\det(D_u)}, \quad (3.36)$$

where determinant $\det(D_u)$ is given by:

$$\operatorname{Re}(\det(D_u)) = -\frac{c_u^+ h^- + c_u^- h^+}{hc_u^- c_u^+} \cos \frac{\omega L_1}{c_u^-} \cos \frac{\omega L_2}{c_u^+} - \frac{c_u^+ h^+ + c_u^- h^-}{hc_u^- c_u^+} \sin \frac{\omega L_1}{c_u^-} \sin \frac{\omega L_2}{c_u^+}, \quad (3.37)$$

$$\operatorname{Im}(\det(D_u)) = \frac{c_u^+ h^- h^+ + c_u^- h^2}{h^2 c_u^- c_u^+} \cos \frac{\omega L_1}{c_u^-} \sin \frac{\omega L_2}{c_u^+} - \frac{c_u^+ h^2 + c_u^- h^- h^+}{hc_u^- c_u^+} \sin \frac{\omega L_1}{c_u^-} \cos \frac{\omega L_2}{c_u^+},$$

and terms $\tilde{\zeta}_u^-(x)$, $\tilde{\zeta}_u^+(x)$, $\tilde{U}_u^-(x)$ and $\tilde{U}_u^+(x)$ are specified by:

$$\begin{aligned} \operatorname{Re}(\tilde{\zeta}_u^-(x)) &= \frac{h^+}{c_u^- h} \left[\frac{c_p^-}{c_u^+} \cos \frac{\omega L_2}{c_u^+} \sin \frac{\omega L_1}{c_p^-} - \sin \frac{\omega L_2}{c_u^+} \cos \frac{\omega L_1}{c_p^-} \right] \cdot \sin \left[\frac{\omega}{c_u^-} (x - L_1) \right] + \\ &+ \frac{h^-}{c_u^- h} \left[\cos \frac{\omega L_2}{c_u^+} \cos \frac{\omega L_1}{c_p^-} + \frac{c_p^-}{c_u^+} \sin \frac{\omega L_2}{c_u^+} \sin \frac{\omega L_1}{c_p^-} \right] \cdot \cos \left[\frac{\omega}{c_u^-} (x - L_1) \right], \end{aligned} \quad (3.38)$$

$$\begin{aligned} \operatorname{Im}(\tilde{\zeta}_u^-(x)) &= -\frac{1}{c_u^-} \left[\cos \frac{\omega L_2}{c_u^+} \cos \frac{\omega L_1}{c_p^-} + \frac{c_p^-}{c_u^+} \sin \frac{\omega L_2}{c_u^+} \sin \frac{\omega L_1}{c_p^-} \right] \cdot \sin \left[\frac{\omega}{c_u^-} (x - L_1) \right] + \\ &+ \frac{h^- h^+}{c_u^- h^2} \left[\frac{c_p^-}{c_u^+} \cos \frac{\omega L_2}{c_u^+} \sin \frac{\omega L_1}{c_p^-} - \sin \frac{\omega L_2}{c_u^+} \cos \frac{\omega L_1}{c_p^-} \right] \cdot \cos \left[\frac{\omega}{c_u^-} (x - L_1) \right], \end{aligned}$$

$$\begin{aligned} \operatorname{Re}(\tilde{\zeta}_u^+(x)) &= -\frac{h^-}{c_u^+ h} \left[\frac{c_p^-}{c_u^-} \cos \frac{\omega L_1}{c_u^-} \sin \frac{\omega L_1}{c_p^-} - \sin \frac{\omega L_1}{c_u^-} \cos \frac{\omega L_1}{c_p^-} \right] \cdot \sin \left[\frac{\omega}{c_u^+} (x - L_2) \right] - \\ &- \frac{h^+}{c_u^+ h} \left[\cos \frac{\omega L_1}{c_u^-} \cos \frac{\omega L_1}{c_p^-} + \frac{c_p^-}{c_u^-} \sin \frac{\omega L_1}{c_u^-} \sin \frac{\omega L_1}{c_p^-} \right] \cdot \cos \left[\frac{\omega}{c_u^+} (x - L_2) \right], \end{aligned} \quad (3.39)$$

$$\begin{aligned} \operatorname{Im}(\tilde{\zeta}_u^+(x)) &= -\frac{1}{c_u^+} \left[\cos \frac{\omega L_1}{c_u^-} \cos \frac{\omega L_1}{c_p^-} + \frac{c_p^-}{c_u^-} \sin \frac{\omega L_1}{c_u^-} \sin \frac{\omega L_1}{c_p^-} \right] \cdot \sin \left[\frac{\omega}{c_u^+} (x - L_2) \right] + \\ &+ \frac{h^- h^+}{c_u^+ h^2} \left[\frac{c_p^-}{c_u^-} \cos \frac{\omega L_1}{c_u^-} \sin \frac{\omega L_1}{c_p^-} - \sin \frac{\omega L_1}{c_u^-} \cos \frac{\omega L_1}{c_p^-} \right] \cdot \cos \left[\frac{\omega}{c_u^+} (x - L_2) \right], \end{aligned}$$

$$\begin{aligned} \operatorname{Re}(\tilde{U}_u^-(x)) &= -\frac{h^- h^+}{h^2} \left[\frac{c_p^-}{c_u^+} \cos \frac{\omega L_2}{c_u^+} \sin \frac{\omega L_1}{c_p^-} - \sin \frac{\omega L_2}{c_u^+} \cos \frac{\omega L_1}{c_p^-} \right] \cdot \sin \left[\frac{\omega}{c_u^-} (x - L_1) \right] + \\ &+ \left[\cos \frac{\omega L_2}{c_u^+} \cos \frac{\omega L_1}{c_p^-} + \frac{c_p^-}{c_u^+} \sin \frac{\omega L_2}{c_u^+} \sin \frac{\omega L_1}{c_p^-} \right] \cdot \cos \left[\frac{\omega}{c_u^-} (x - L_1) \right], \end{aligned} \quad (3.40)$$

$$\begin{aligned} \operatorname{Im}(\tilde{U}_u^-(x)) &= \frac{h^-}{h} \left[\cos \frac{\omega L_2}{c_u^+} \cos \frac{\omega L_1}{c_p^-} + \frac{c_p^-}{c_u^+} \sin \frac{\omega L_2}{c_u^+} \sin \frac{\omega L_1}{c_p^-} \right] \cdot \sin \left[\frac{\omega}{c_u^-} (x - L_1) \right] - \\ &- \frac{h^+}{h} \left[\frac{c_p^-}{c_u^+} \cos \frac{\omega L_2}{c_u^+} \sin \frac{\omega L_1}{c_p^-} - \sin \frac{\omega L_2}{c_u^+} \cos \frac{\omega L_1}{c_p^-} \right] \cdot \cos \left[\frac{\omega}{c_u^-} (x - L_1) \right], \end{aligned}$$

$$\begin{aligned} \operatorname{Re}(\tilde{U}_u^+(x)) &= -\frac{h^- h^+}{h^2} \left[\frac{c_p^-}{c_u^-} \cos \frac{\omega L_1}{c_u^-} \sin \frac{\omega L_1}{c_p^-} - \sin \frac{\omega L_1}{c_u^-} \cos \frac{\omega L_1}{c_p^-} \right] \cdot \sin \left[\frac{\omega}{c_u^+} (x - L_2) \right] + \\ &+ \left[\cos \frac{\omega L_1}{c_u^-} \cos \frac{\omega L_1}{c_p^-} + \frac{c_p^-}{c_u^-} \sin \frac{\omega L_1}{c_u^-} \sin \frac{\omega L_1}{c_p^-} \right] \cdot \cos \left[\frac{\omega}{c_u^+} (x - L_2) \right], \end{aligned} \quad (3.41)$$

$$\begin{aligned} \operatorname{Im}(\tilde{U}_u^+(x)) &= -\frac{h^+}{h} \left[\cos \frac{\omega L_1}{c_u^-} \cos \frac{\omega L_1}{c_p^-} + \frac{c_p^-}{c_u^-} \sin \frac{\omega L_1}{c_u^-} \sin \frac{\omega L_1}{c_p^-} \right] \cdot \sin \left[\frac{\omega}{c_u^+} (x - L_2) \right] + \\ &+ \frac{h^-}{h} \left[\frac{c_p^-}{c_u^-} \cos \frac{\omega L_1}{c_u^-} \sin \frac{\omega L_1}{c_p^-} - \sin \frac{\omega L_1}{c_u^-} \cos \frac{\omega L_1}{c_p^-} \right] \cdot \cos \left[\frac{\omega}{c_u^+} (x - L_2) \right]. \end{aligned}$$

The general solution for free oscillations with angular frequency ω , as a function of time and space (real form) and up to arbitrary amplitude A and phase φ , is:

$$X^\pm(x, t) = \begin{bmatrix} U_p^\pm(x, t) \\ \zeta_\rho^\pm(x, t) \\ U_u^\pm(x, t) \\ \zeta_u^\pm(x, t) \end{bmatrix} = \operatorname{Re} \left(A e^{i\varphi} \begin{bmatrix} U_p^\pm(x) \\ \zeta_\rho^\pm(x) \\ U_u^\pm(x) \\ \zeta_u^\pm(x) \end{bmatrix} \cdot e^{i\omega t} \right). \quad (3.42)$$

This model was also combined with three parameterizations of the Adriatic, as described in the previous section. The most important difference arising from the model with radiation boundary conditions for internal mode is the progressive character of waves on thermocline. Amplification of tidal signal occurs due to the same reasons as in the previous case, i.e. due to the ratio between speed of the surface and speed of the internal waves. However, this model is also sensitively dependent on model parameters – depths of shallow and deep region and discontinuity coordinate.

The coordinate corresponding to the position of Lastovo is also very important for the results of the model, having in mind that surface wave is standing wave, and internal wave has a progressive character, with phase depending upon position. For this reason, matching phases between surface oscillations and thermocline oscillations will occur only at a certain point, its position depending on the speed of internal waves. The best results were found for Sterneck's approximation, with spacing equal to 20.5 km, and these results are presented in Figures 22 – 23.

Figure 22 shows space-time distribution of surface elevation for a distance extending 100 km from the origin in both directions, according to equations (3.27a) and (3.27c). The time interval of 48 h was analyzed, with natural frequency of the fundamental mode related to above mentioned Adriatic parameterization. Standing wave can be noticed, with larger amplitudes obtained to the left of the origin, which corresponds well with the results in the previous section (Figures 19 to 21). Space-time distribution of thermocline elevation (Figure 23) was calculated by including terms (3.27a), (3.27c) and (3.35) into equation (3.19d), and by taking into account fundamental frequency for Sterneck's approximation, with spacing of 20.5 km. Thermocline oscillations are amplified with respect to surface oscillations and internal wave is progressive on both sides of the origin. When Lastovo position is analyzed ($x = -43$ km), it can be seen that surface and thermocline oscillations are in phase at that position, with amplification factor of about 50 (Figure 24). These results accord well with temperature data measured at Lastovo in June 2001 (Mihanovic, 2005). Still, small change of depths, coordinate of discontinuity and Lastovo position can significantly change the phase and amplification for such an approximation.

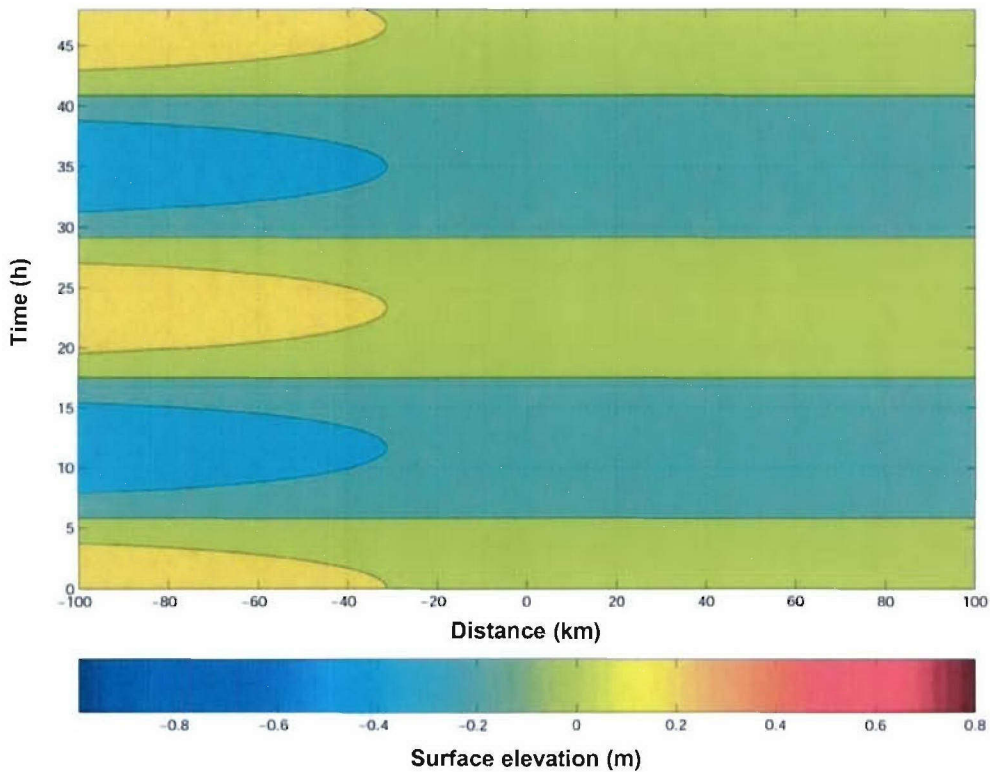


Figure 22. Space-time distribution of surface elevation for a distance extending 100 km from the origin in both directions and time interval of 48 h (parameterization of the Adriatic according to Sterneck, with spacing of 20.5 km).

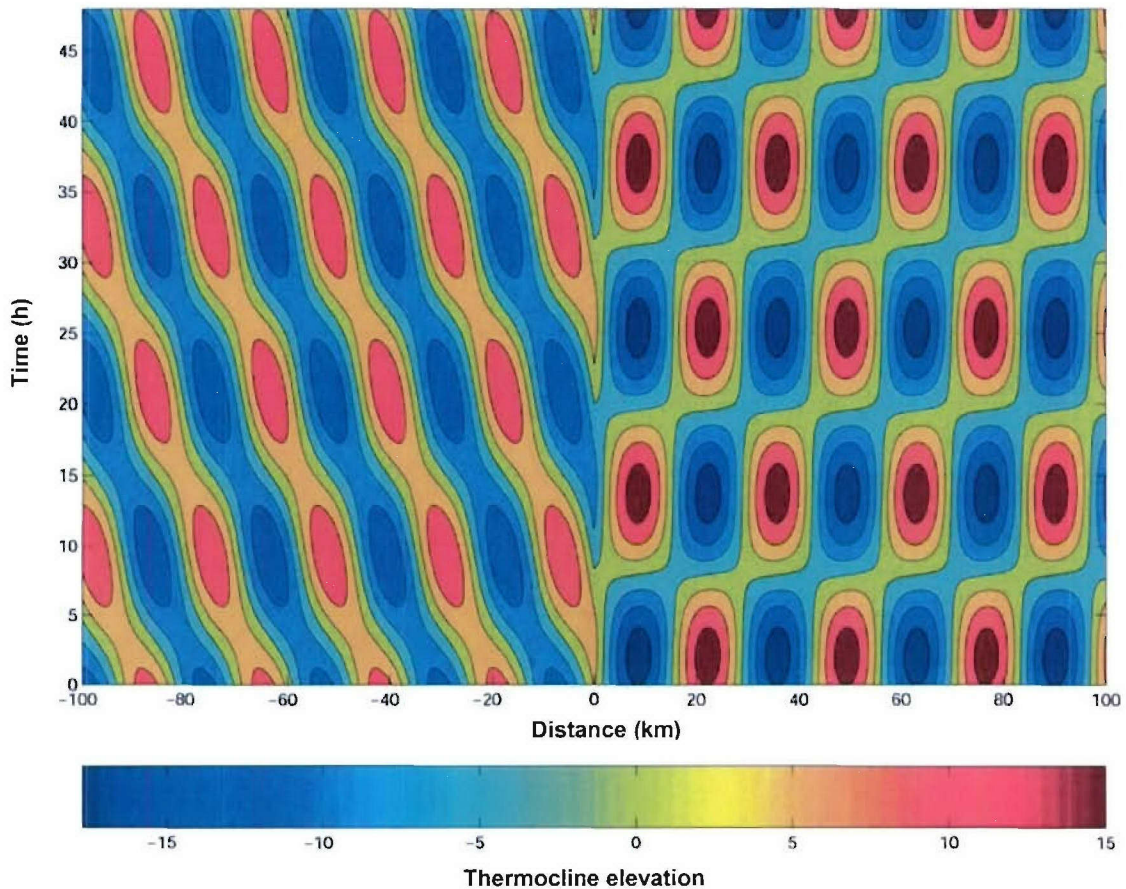


Figure 23. Space-time distribution of thermocline elevation for a distance extending 100 km from the origin in both directions and time interval of 48 h (parameterization of the Adriatic according to Sterneck, with spacing of 20.5 km).

3. 4. Discussion

Two-layer analytical model represents a starting point for theoretical study of the generation of internal tides. Its application to the Adriatic enables one to acquire fundamental understanding of physical processes important for amplification of thermocline oscillations. It also paves the way to future examination of internal tides with more advanced theoretical models, which would encompass cross-basin changes of barotropic flow and realistic density distribution. Another important aspect is its relevance for development of numerical models.

This report examines the results of two analytical models based on two-layer fluid approximation, with a rapid depth change at the shelf break. The two models originate in the same initial equations and utilize the same boundary conditions at depth discontinuity. Boundary conditions include elevation continuity in the surface and bottom layer, as well as flow continuity in the entire water column and in each layer. The main difference between analyzed models arises from assumption about the nature of the surface wave, which represents barotropic tide of diurnal period.

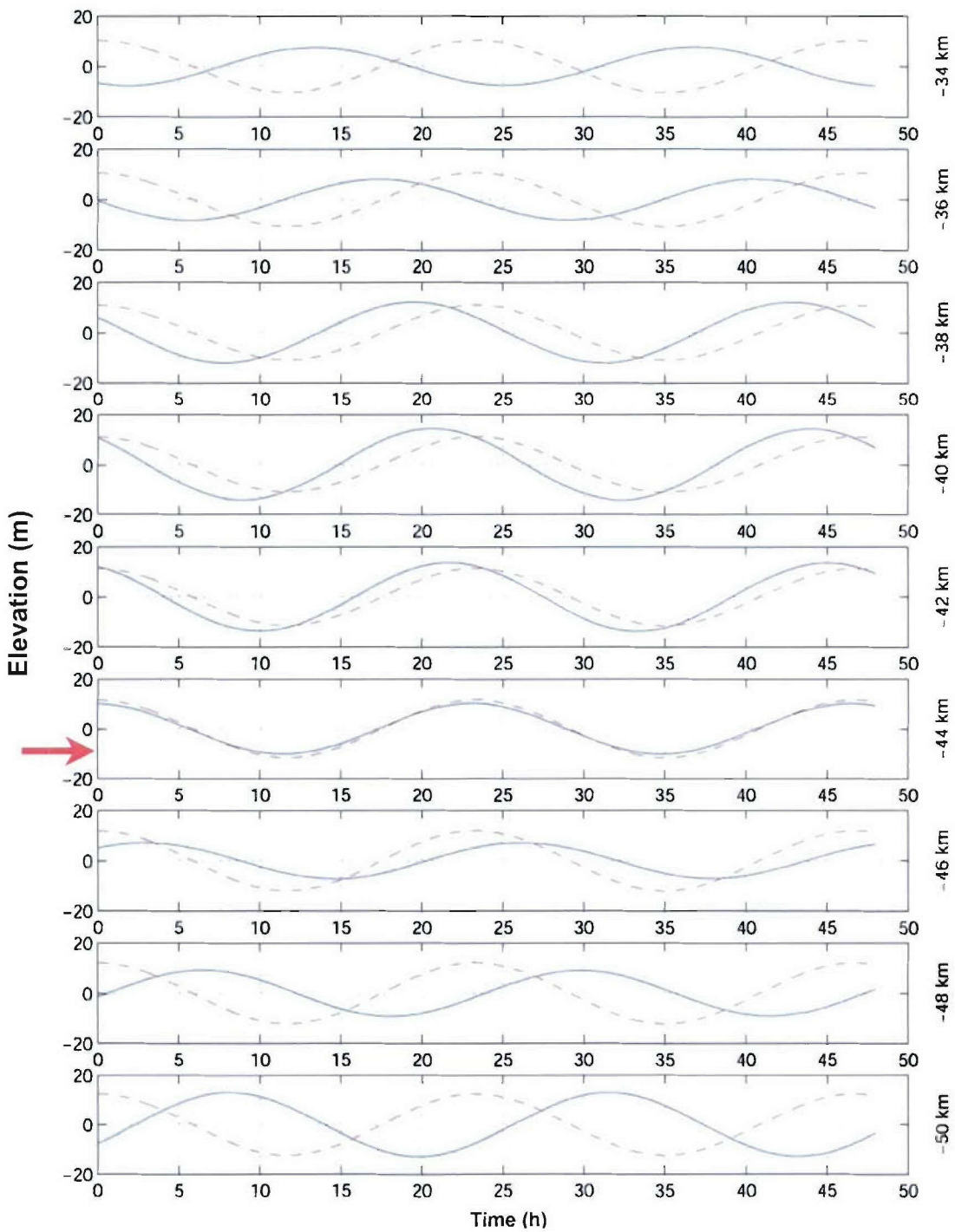


Figure 24. Time series of surface elevation multiplied by 50 (red line) and time series of thermocline elevation (blue line) at a distance of 34 to 50 km from the origin towards the closed end of the basin (parameterization of the Adriatic according to Sterneck, with spacing of 20.5 km). Graph representing approximate position of Lastovo ($x = -43$ km) is denoted by an arrow.

The first model presumes that K1 tide in the Adriatic is progressive barotropic wave propagating from deep into shallow water. It is then partly reflected and partly transmitted at topography discontinuity, thus generating reflected and transmitted internal waves. The results of the model for depth parameters in the shallow and deep region valid for the Adriatic, and for thermocline depth and stratification observed in June 2001, are close to the results determined from the surface and thermocline elevations measured in the same interval. They are also comparable to the ratio of amplitudes calculated by harmonic analysis of surface elevation at Dubrovnik and thermocline elevation at Lastovo for June 2001. Amplitude of thermocline oscillations is proportional to surface oscillations and thermocline depth, and inversely proportional to density difference between the surface and bottom layer. By increasing the depth of shallow region amplification of thermocline oscillations is decreased, whereas an increase of deep region depth has an opposite effect. These results are in agreement with previous findings from similar two-layer analytical models. However, the progressive character of surface wave presumed in this models means that elevation and velocity oscillations are in phase, which is not the case in a wider Lastovo area, or in accordance with standing wave character of diurnal tide in the Adriatic. Harmonic analysis of sea currents in the Lastovo channel (July 1990) shows that diurnal tidal currents lead elevation oscillations by about 90°. This implies that surface standing wave is more suitable for describing the characteristics of K1 tide than is surface progressive wave.

Therefore, another analytical model is developed, which also specifies conditions at the basin boundaries, thus enabling examination of surface standing wave and its influence on thermocline oscillations. In the first case, classical boundary conditions for the surface and internal mode are presumed at the closed and open end of the basin. Model results demonstrate sensitive dependence on the values of parameters defining the Adriatic (depths of shallow and deep region, distance of the boundaries from the depth discontinuity). Since the solutions for the surface and boundary layer are standing waves, and lengths of internal waves lie between 20 and 40 km, at some points along the Adriatic transect thermocline and surface oscillations are in phase and at other points they are opposed in phase. Depending on parameterization, Lastovo could be in either of these two areas, and moreover it could be positioned close to the nodal point. If it were at the nodal point, no significant amplification of thermocline variability would be recorded. When radiation boundary conditions are imposed for internal mode, thermocline wave has progressive character. This is closer to basic ideas about generation of internal tides, which state that barotropic flow changes on topography discontinuity generate internal waves that propagate towards shallow and deep regions of the analyzed basin (*Baines, 1982*). However, the sensitive dependence of the model on small changes in parameters defining the Adriatic, especially on depths of the shallow and deep region, is still present. The phase locking of the surface and thermocline elevation as observed at Lastovo is obtained at individual points only, depending on their distance from the origin (depth discontinuity) and the speed of internal wave. The best results are obtained for the coarsest Adriatic approximation, because Lastovo position in that case matches position of the point at which internal wave in the shallow region has the same phase as the surface standing wave.

Implementation of the models described enables one to get some insight into physical processes responsible for generation of internal tides in the Adriatic. It also allows comparison of model results with the data. Limitations of models are detected and discussed, being related to the character of surface wave in the first model, to the Adriatic parameterizations and boundary conditions in the second model. Nevertheless, it is hoped that the present findings could provide a starting point for a further investigation of the Adriatic internal tides.

4. SUMMARY AND CONCLUSION

Analysis of historical data has shown that in the middle Adriatic area seasonal variations of main atmospheric parameters such as solar radiation, wind, air temperature and precipitation cause pronounced seasonality of heat and water fluxes between the atmosphere and the sea. Strong cyclonic activity, especially in the colder part of the year, causes different weather types to occur, with frequent exchange of Sirocco and Bora events. During summer, this area is under the influence of subtropical high-pressure belt, and consequently warm and dry weather conditions prevail with well-developed sea-land breeze system. Seasonal cycle of sea temperature at various depths of the Split-Gargano transect points to isothermal conditions in late autumn and winter and rather small changes at 100 meters where the temperature does not fall below 12°C. In deeper layers annual maximum is lagging the surface one, whereas minimum at all depths occurs within the same month. Sea temperature variations in a particular month are maximal in the surface layer, with the variability decreasing as the depth increases. Seasonal cycle of salinity shows that the salinity increases with depth throughout the year. In the surface layer, down to 10 meter depth, there are two minima of salinity, in May and July. At a 20 meter depth the second minimum disappears whereas the summer-autumn maximum is well visible. Large salinity fluctuations, maximal in the surface layer, are apparent within a month.

A simple two-layer analytical model with step-like topography has been built as a first step in theoretical analysis of internal tides. Basic assumptions underlying such a model are fulfilled in the vicinity of the Palagruza Sill. The model aims at understanding origin of internal tides and it is based on separate equations for the barotropic and baroclinic mode of oscillations in the two-layer fluid contained in rectangular channel. Initially, the model was solved with an assumption of progressive surface wave. It resulted in the relationship between thermocline oscillations on one hand and amplitude of barotropic tide, depth of the shelf and deep-sea regions, thermocline depth and density difference between the bottom and surface layers on the other. The amplitude ratio calculated by the model, using physical parameters (thermocline depth and density difference) corresponding to June 2001, was around 10, which is in agreement with the empirical results. However, the phase difference between surface elevation and currents from this model is not appropriate for diurnal barotropic tide in the Adriatic, which shows features similar to the standing surface wave. Therefore, a two-layer analytical model for the standing surface wave was developed, in which the Adriatic was approximated by a semi-enclosed basin with a step-like topography. This model covered two different cases. In the first classical boundary conditions were imposed for the surface and internal mode at the closed and open end of the basin, giving standing wave both at the surface and at the thermocline. In the second case radiation boundary conditions were imposed for the internal mode, resulting in progressive character of the thermocline wave. Both models succeeded in capturing the basics of internal tide generation, as it occurs under the influence of changes in barotropic flow at the shelf break. However, they also demonstrated sensitive dependence on the parameters that define the Adriatic basin (deep sea and shelf region depths, depth discontinuity coordinate, position of observation point in the respective coordinate system).

The results from the present report have helped to define the precise positions of the ITHACA measurement points. They are shown in Figure 25, whereas the coordinates of the ADCP, thermistor and CTD stations are given in Table 3. The stations were selected so as to enable hypotheses stated in this report to be tested, but also with the aim of complementing stations that will be occupied in the framework of another project planned for the same area and time (Dynamics of the Adriatic in Real Time – DART). Let it be added that the instruments needed for the present project (ADCPs, thermistors, CTD probes, meteorological package, tide gauge) are prepared for the start of the experimental work in February 2006.

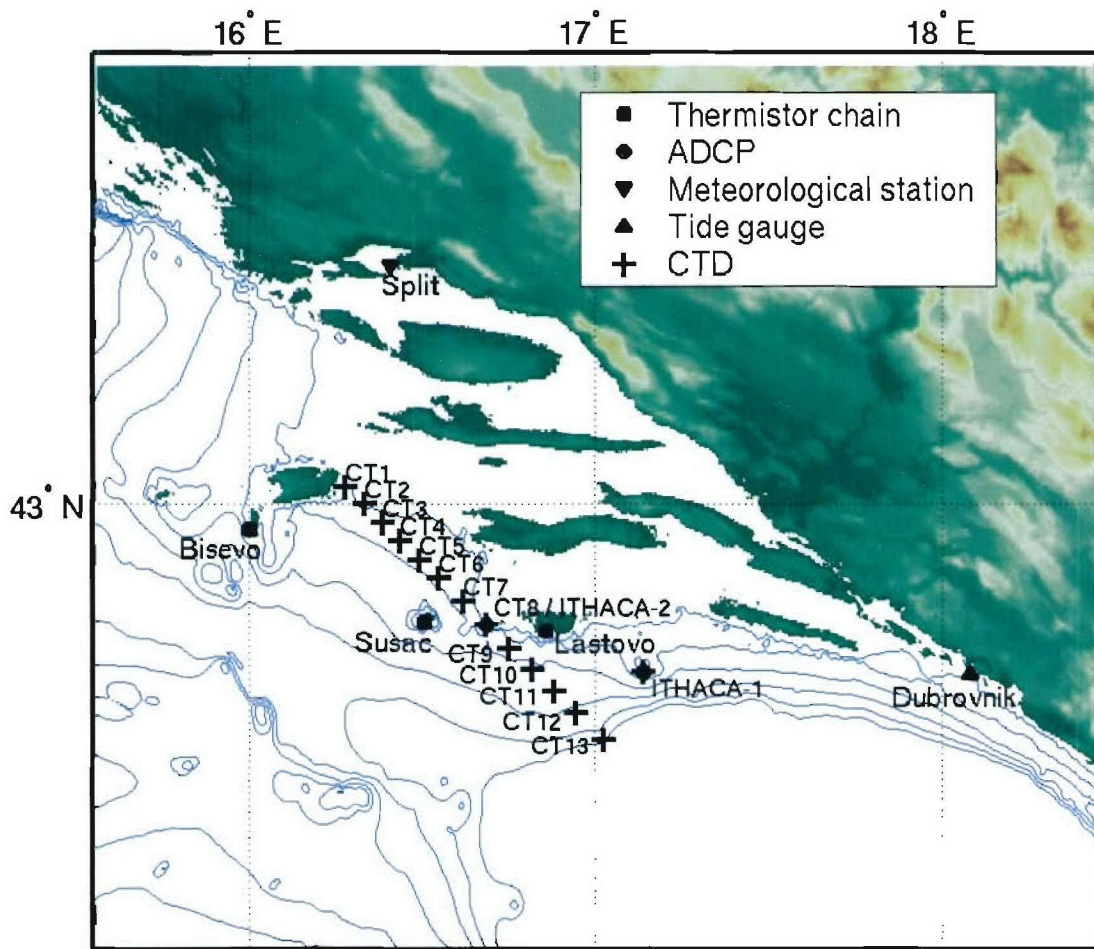


Figure 25. Position of stations to be occupied in the framework of ITHACA project.

Table 3. Basic information on the ADCP, thermistor and CTD stations to be occupied in the framework of ITHACA project.

Station	Instruments	Latitude	Longitude	Approx. depth (m)
ITHACA-1	ADCP	42.64553	17.14057	106
ITHACA-2	ADCP	42.74562	16.68553	102
BISEVO	THERMISTORS	42.95337	16.01276	/
SUSAC	THERMISTORS	42.75633	16.51851	/
LASTOVO	THERMISTORS	42.72775	16.90049	/
CT1	CTD	43.03689	16.27861	95
CT2	CTD	43.00000	16.33333	105
CT3	CTD	42.96088	16.38643	110
CT4	CTD	42.92200	16.43593	115
CT5	CTD	42.88311	16.49072	115
CT6	CTD	42.84422	16.54729	110
CT7	CTD	42.79650	16.61799	115
CT8	CTD	42.74562	16.68553	102
CT9	CTD	42.69574	16.75233	135
CT10	CTD	42.65155	16.81596	145
CT11	CTD	42.60559	16.88136	160
CT12	CTD	42.55963	16.94323	175
CT13	CTD	42.50307	17.02277	190

Acknowledgement

The work reported here was supported by the USA Office of Naval Research (award No. N00014-05-1-0698) and the Croatian Ministry of Science, Education and Sports (contract No. 3/2005).

REFERENCES

- Baines, P. G. (1982): On internal tide generation models, *Deep-Sea Research*, **29**, 307-338.
- Baines, P. G. (1986): Internal tides, internal waves and near internal motions, In: Mooers, C. N. K. (Ed.): *Baroclinic Processes on Continental Shelves*, American Geophysical Union, Washington, D. C., 19-31.
- Buljan, M. (1974): Basic characteristics of the Adriatic Sea as a production basin, *Acta Adriatica*, **16**, 31-62.
- Buljan, M., Zore-Armanda, M. (1976): Oceanographical properties of the Adriatic Sea, *Oceanography and Marine Biology: An Annual Review*, **14**, 11-98.
- Cerovecki, I. (1992): *Decay of Standing Waves in the Adriatic Sea (in Croatian)*, M. Sc. Thesis, University of Zagreb, Zagreb, 105 pp.
- Csanady G. T. (1971): Baroclinic boundary currents and long edge-waves in basins with sloping shores, *Journal of Physical Oceanography*, **1**, 92-104.
- Gerkema, T. (1996): A unified model of the generation and fission of internal tides in a rotating ocean, *Journal of Marine Research*, **54**, 421-450.
- Gill, A. E. (1982): *Atmosphere-Ocean Dynamics*, Academic Press, Orlando, 662 pp.
- Grbec, B. (1998): Influence of climatic changes on oceanographic properties of the Adriatic Sea, *Acta Adriatica*, **38**, 3-29.
- Grbec, B., Morovic, M. (1997): Seasonal thermohaline fluctuations in the middle Adriatic Sea, *Il Nuovo Cimento C*, **20**, 561-576.
- Grbec, B., Beg Paklar, G., Morovic, M. (1997): On the evaporation problem over the Adriatic Sea, *Acta Adriatica*, **38**, 69-77.
- Grbec, B., Morovic, M., Zore-Armanda, M. (2003): Mediterranean Oscillation and its relationship to salinity fluctuation in the Adriatic Sea, *Acta Adriatica*, **44**, 61-76.
- Guizien, K., Barthélemy E., Inall, M. E. (1999): Internal tide generation at a shelf break by an oblique barotropic tide: observations and analytical modeling, *Journal of Geophysical Research*, **104 (C7)**, 15655-15668.
- Holloway, P. E. (1983): Internal tides on the Australian North-West Shelf: a preliminary investigation, *Journal of Physical Oceanography*, **13**, 1357-1370.
- Holloway, P. E. (1987): Internal hydraulic jumps and solitons at a shelf-break region on the Australian North West Shelf, *Journal of Geophysical Research*, **92 (C5)**, 5405-5416.
- Huthnance, J. M. (1989): Internal tides and waves near the continental shelf edge, *Geophysical and Astrophysical Fluid Dynamics*, **48**, 81-106.
- Leder, N. (2002): Wind-induced internal wave dynamics near the Adriatic shelf break, *Continental Shelf Research*, **22**, 445-463.
- Leder, N., Smircic, A., Grzetic, Z., Grbec, B., Vilibic, I. (1996): Dynamic characteristics of the Palagruza Sill area, In: Hodzic, M. (Ed.): *Palagruza – The Pearl of the Adriatic*, Hrvatska pomorska meteoroloska sluzba, Split, 339-343.
- Loncar, E., Bajic, A. (1994): Weather types in Croatia (in Croatian), *Hrvatski meteoroloski casopis*, **29**, 31-41.
- Matic, F. (2005): *Air-Sea Interaction in the Split, Brac and Neretva Channels (in Croatian)*, M. Sc. Thesis, University of Zagreb, Zagreb, 71 pp.
- Maze, R. (1987): Generation and propagation of non-linear internal waves induced by tide over a continental slope, *Continental Shelf Research*, **7 (9)**, 1079-1104.
- Mihanovic, H. (2005): *Internal Tides in the Adriatic (in Croatian)*, M. Sc. Thesis, University of Zagreb, Zagreb, 118 pp.

- Miles, J. W. (1974): On Laplace's tidal equations, *Journal of Fluid Dynamics*, **66**, 241-260.
- Mosseti, F., Purga, N. (1983): Free oscillations of the Adriatic Sea. Comparison and discussion of some results by old models and recent experimental investigations, *Bollettino di Oceanologia Teorica ed Applicata*, **1**, 279-310.
- New, A. L., Da Silva J. C. B. (2002): Remote-sensing evidence for the local generation of internal soliton packets in the central Bay of Biscay, *Deep-Sea Research I*, **49**, 915-934.
- Orlic, M. (1988): *Oscillations of the Inertia Period in the Adriatic Sea – Analysis of the Phenomenon and Formulation of Two-Dimensional Models (in Croatian)*, Ph. D. Thesis, University of Zagreb, Zagreb, 164 pp.
- Orlic, M., Gacic, M., LaViolette, P. (1992): The currents and circulation of the Adriatic Sea, *Oceanologica Acta*, **15**, 109-124.
- Penzar, B. (1967): Some characteristics of weather types in the Adriatic (in Croatian), *Hidrografski godisnjak*, **67**, 99-124.
- Prinsenbergh, S. J., Rattray, M. (1975): Effects of continental slope and variable Brunt-Väisälä frequency on the coastal generation of internal tides, *Deep-Sea Research*, **22**, 251-263.
- Rattray, M. (1960): On the coastal generation of internal tides, *Tellus*, **12**, 54-62.
- Sherwin, T. J., Taylor, N. K. (1990): Numerical investigations of linear tide generation in the Rockall Trough, *Deep-Sea Research II*, **37**, **10**, 1595-1618.
- Sherwin, T. J., Vlasenko, V. I., Stashchuk, N., Gus Jeans, D. R., Jones, B. (2002): Along-slope generation as an explanation for some unusually large internal tides, *Deep-Sea Research I*, **49**, 1787-1799.
- Sterneck, R. (1919): Die Gezeitenerscheinungen in der Adria – II. Teil – Die theoretische Erklärung der Beobachtungstatsachen, *Denkschriften der Akademie der Wissenschaften in Wien*, **96**, 277-324.
- Vilibic I., Grbec, B., Supic, N. (2004): Dense water generation in the north Adriatic in 1999 and its recirculation along the Jabuka Pit, *Deep Sea Research I*, **51**, 1475-1474.
- Zore-Armanda, M. (1963): Les masses d'eau de la mer Adriatique, *Acta Adriatica*, **10**, 1-94.
- Zore-Armanda, M. (1968): *The System of Currents in the Adriatic Sea*, FAO, Rome, 48 pp.
- Zore-Armanda, M. (1969a): Temperature relations in the Adriatic Sea, *Acta Adriatica*, **13**, 1-50.
- Zore-Armanda, M. (1969b): Water exchange between the Adriatic and the Eastern Mediterranean, *Deep-Sea Research*, **16**, 171-178.
- Zore-Armanda, M. (1969c): Origine possible des fluctuations de la salinité de l'eau de la mer Adriatique, *Rapports Commission Internationale pour l'Exploration Scientifique de la Mer Méditerranée*, **19**(4), 719-722.
- Zore-Armanda, M., Bone, M. (1987): The effect of bottom topography on the current system of the open Adriatic Sea, *Bollettino di Oceanologia Teorica ed Applicata*, **5**, 3-18.
- Zore-Armanda, M., Grbec, B., Morovic, M. (1999): Oceanographic properties of the Adriatic Sea - a point of view, *Acta Adriatica*, **40**, 39-54.

REPORT DOCUMENTATION PAGE

*Form Approved
OMB No. 0704-0188*

The public reporting burden for this collection of information is estimated to average 1 hour per response, including the time for reviewing instructions, searching existing data sources, gathering and maintaining the data needed, and completing and reviewing the collection of information. Send comments regarding this burden estimate or any other aspect of this collection of information, including suggestions for reducing the burden, to Department of Defense, Washington Headquarters Services, Directorate for Information Operations and Reports (0704-0188), 1215 Jefferson Davis Highway, Suite 1204, Arlington, VA 22202-4302. Respondents should be aware that notwithstanding any other provision of law, no person shall be subject to any penalty for failing to comply with a collection of information if it does not display a currently valid OMB control number.

PLEASE DO NOT RETURN YOUR FORM TO THE ABOVE ADDRESS.

1. REPORT DATE (DD-MM-YYYY) 31-12-2005		2. REPORT TYPE Performance / technical report		3. DATES COVERED (From - To) 12-04-2005 - 31-12-2005	
4. TITLE AND SUBTITLE Internal Tidal Hydrodynamics and Ambient Characteristics of the Adriatic (ITHACA) - Report on the First Year of Work				5a. CONTRACT NUMBER /	
				5b. GRANT NUMBER N00014-05-1-0698	
				5c. PROGRAM ELEMENT NUMBER /	
6. AUTHOR(S) Orlic, Mirko; Beg Paklar, Gordana; Dadic, Vlado; Leder, Nenad; Grbec, Branka; Mihanovic, Hrvoje; Pasaric, Miroslava; Pasaric, Zoran.				5d. PROJECT NUMBER 05PR08927-00	
				5e. TASK NUMBER /	
				5f. WORK UNIT NUMBER /	
7. PERFORMING ORGANIZATION NAME(S) AND ADDRESS(ES) University of Zagreb, Horvatovac bb, 10000 Zagreb, Croatia				8. PERFORMING ORGANIZATION REPORT NUMBER /	
9. SPONSORING/MONITORING AGENCY NAME(S) AND ADDRESS(ES) Office of Naval Research, 875 N. Randolph St., One Liberty Center, Arlington VA 22203-1995, USA				10. SPONSOR/MONITOR'S ACRONYM(S) ONR	
				11. SPONSOR/MONITOR'S REPORT NUMBER(S) /	
12. DISTRIBUTION/AVAILABILITY STATEMENT Approved for public release					
13. SUPPLEMENTARY NOTES /					
14. ABSTRACT Analysis of historical data has shown that in the middle Adriatic area strong cyclonic activity supports different weather types in winter, with frequent exchange of Sirocco and Bora events. During summer, this area is under the influence of subtropical high-pressure belt and consequently warm and dry weather conditions prevail. Sea temperatures at various depths of the Split-Gargano transect are characterized by isothermal conditions in late autumn and winter and rather small changes at 100 meters where the temperature does not fall below 12°C. Salinities are minimal in the surface layer, most so in May and July. Analytical modeling, based on separate equations for the barotropic and baroclinic modes of the two-layer fluid contained in rectangular channel with a step-like topography, has allowed for both the progressive and standing surface waves. It pointed to the relationship between amplitude of internal tides on one hand and amplitude of surface tides, depth of the shelf and deep-sea regions, pycnocline depth and density difference between the two layers on the other. The results described in the present report have helped to define the precise positions of the ITHACA measurement points and thus to prepare for the start of experimental work in February 2006.					
15. SUBJECT TERMS Internal tides, surface tides, thermohaline properties, meteorological conditions, Adriatic					
16. SECURITY CLASSIFICATION OF:			17. LIMITATION OF ABSTRACT SAR	18. NUMBER OF PAGES 56	19a. NAME OF RESPONSIBLE PERSON Mirko Orlic
a. REPORT U	b. ABSTRACT U	c. THIS PAGE U			19b. TELEPHONE NUMBER (Include area code) +385-1-460-5900